**Award Number: G12AP20082**

# Estimating site response by constraining shallow velocity structure with local P waves in the Central and Eastern United States

**FINAL TECHNICAL REPORT**

**July 31, 2013**

Sidao Ni and Paul Somerville*

URS Group, Inc.

915 Wilshire Boulevard
Los Angeles CA 90017

Tel: 213.996.2200
Fax: 213.996.2290

*Email: paul.somerville@urs.com

Research supported by the U.S. Geological Survey (USGS), Department of the Interior, under award number G12AP20082. The views and conclusions contained in this document are those of the authors and should not be interpreted as necessarily representing the official policies, either expressed or implied, of the U.S. Government.

**Abstract**

USARRAY and ANSS seismic stations provide an invaluable waveform dataset for studying ground motion attenuation in the Central United States. However, the dataset is useful only after site effects of each station are well understood. Since there are so many stations in USARRAY and ANSS, it may be costly to accurately determine sub-surface velocity structure beneath every station geophysical exploration techniques involving arrays, such as ReMi and SASW. It would be more economical to estimate the site effects with waveforms (either from ambient noise or from seismic events) recorded at the seismic stations. Such approaches have been widely applied, but most of them involve the frequency dependent ratio between the horizontal and vertical component of either ambient noise (HV method) or S waves from earthquakes (HVSR method). Similarly, the horizontal component of P waves can also be used to infer sub-surface velocity structure. From theoretical derivation, it is demonstrated that the ratio of radial to vertical P waves is mostly sensitive to sub-surface shear velocity, and not sensitive to sub-surface density and P velocities, so the radial/vertical ratio of the P wave is a good indicator of subsurface shear velocity. Moreover, for the case of soft soil above hard bedrock, the S wave is generated from the P wave by the sharp velocity contrast between soil and bedrock (referred as Ps hereafter). The amplitude of Ps and its time lag after the P wave provide extra constraints on subsurface shear velocity. When the source duration of a local earthquake is short enough, the direct P wave and the Ps wave can be observed on the radial component while only the P wave is clear on vertical component. Therefore, the subsurface velocity structure can be estimated using an approach similar to teleseismic P receiver functions, but at much smaller scale and higher frequency. We developed an automatic method for measuring the ratio of radial and vertical components of initial P waves, and used the ratios to estimate subsurface shear velocity structures for USARRAYS and ANSS stations which record M3+ local earthquakes in the Central and Eastern United States. We also developed a method of local P receiver function that resolves subsurface shear velocity profiles, and showed that the subsurface velocity structure inferred from P waves for station OLIL is consistent with results from ReMi methods The method is applied to study site characterization at ANSS station CBN, which is the permanent station recording the strongest ground motion for the 2011 Virginia earthquake. Therefore, the initial portion of local P waves are useful in constraining subsurface shear velocity structure, and thus helpful for site characterization.

# Part I

# Theoretical Framework for Estimating Subsurface Shear Velocity with the Radial to Vertical Ratio of Local P Waves

## 1. Introduction

In contrast to the western United States where seismicity is high and seismic networks are dense, the Central and Eastern United States (CEUS) is covered with sparse seismic networks. The relatively low seismicity in the CEUS has also lead to a limited dataset of waveform data from local earthquakes, hindering the development of reliable ground motion prediction equations in the CEUS. This situation has been changing with the Earthscope Transportable Array (USARRAY) program which started installing about 1000 broadband and short period stations in the CEUS starting in 2009, and will fully cover the CEUS soon. Such large numbers of stations provide a rich dataset for ground motion studies in the United States. Also, the increasing number of ANSS broadband stations with high sampling rate substantially augments the waveform data.

Site responses at each seismic station need to be obtained before the waveform data can be used for ground motion studies. For example, Boore (2003) and Atkinson and Boore (2006) find that site amplification needs to be taken into account for ground motion modeling in eastern North America, especially for high frequencies. Site response is basically controlled by the subsurface shear velocity profile, and the velocity structure of the top tens to hundreds of meters is particularly important (Boore, 2006; Wald and Mori, 2000). Therefore an essential part of site response modeling is determining subsurface velocity structure.

A detailed review of methods for determining subsurface velocity structure was made by Boore (2006). Theoretically, invasive methods such as borehole logging provide the most accurate measurement of velocity structure, but their cost prohibits extensive application in site response studies. Noninvasive geophysical exploration methods are more often used in determining shallow velocity structure, and these include SASW, MASW and ReMi (Louie 2001; Odum et al., 2010; Stephenson et al., 2005). These noninvasive methods typically employ arrays of seismic receivers in deriving either travel time curves of body waves or dispersion curves of surface waves excited by a man-made source or by natural ambient noise. Because of the close

spacing between seismic receivers, array-based methods can provide high resolution velocity profiles at relatively low cost.

However, array-based geophysical methods can only be conveniently applied to a relatively small number of sites because they are costly and time consuming. It would be very challenging to perform subsurface structure studies using array-based geophysical exploration methods for all the 400+ stations in the USSARY and ANSS. Instead, methods such as HV and HVSR only require waveforms at single stations from recordings of ambient noise or local S waves. Since all the USARRAY and ANSS stations provide continuous waveforms, these single station-based methods can be readily applied to infer site responses.

Both the HV and HVSR methods use the spectral ratio between horizontal and vertical components as a proxy of site response. The difference between HV and HVSR is that the HV method is applied to the waveform of ambient noise while HVSR is applied to S waves from local earthquakes. Though it is associated with some controversy (Lachet and Bard, 1994; Yuncha and Luzon, 2000; Langston et al., 2009), the HV method is widely applied because seismic stations record ambient noise most of the time (Lozano, et al., 2008). The HV method assumes that the ambient noise consists mostly of Rayleigh waves, and therefore the ellipticity of particle motion can be used to infer subsurface response (Nakamura, 1989, 2000). Some studies directly use the spectral ratio of HV as a proxy for site amplification (Read et al, 2008). There are also efforts to invert the subsurface velocity profile from the HV ratio (Arai and Tokimatsu, 2004). The HVSR method is also widely adopted in modeling site response, but requires S waveforms from local earthquakes (Lermo and Chávez-García, 1993). For example, earthquakes in the magnitude range of 2.0-3.8 have been used in modeling site responses for POLARIS stations (Read et al., 2008).

## 2. Theory for estimating shallow shear velocity from local P waveforms

As for S waves, P waves should be able to provide constraints on sub-surface structure. For the case of a layer of unconsolidated sediments over bedrock, various converted seismic phases are observed (Sp, or Ps), and are used to improve estimates of the velocity structure in the sediments (Chen et al, 1996; Langston, 2003). The same approach can be used to model near surface structure (tens to hundreds of meters), when the first tenths of a second of the P waveforms are examined. In Figure 1.1A, the ray paths of the P wave and a converted phase (Ps)

are displayed. As most earthquakes occur in crystalline basement where seismic velocities are high, and most stations are situated on material of lower velocities, the incidence angles of P and Ps near the seismic station are typically much smaller than the takeoff angle at the earthquake. Thus intuitively, the P wave is weaker on the radial component than on the vertical component because of the steeper ray path of the P wave, and Ps is stronger on the radial component because its polarization is perpendicular to the ray path.

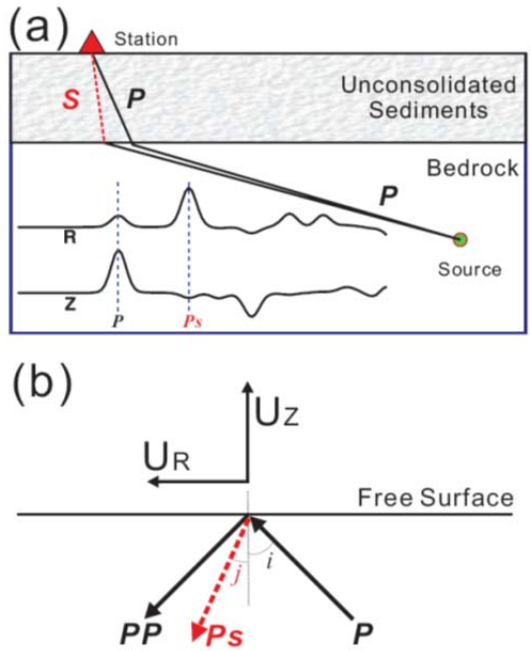


Figure 1.1. Schematic rays showing interaction of the P wave and subsurface structure (a) and the free surface (b). The radial (top) and vertical (bottom) waveforms are shown in Panel a.

Due to the interaction of incoming P and S waves with the free surface, the actual particle motion recorded by a seismic station is different from that of waves propagating in a whole space. From Aki and Richards (2002), the particle motions of incoming P waves and S waves are described by equation (1) and equation (2) respectively, where $U_R$, $U_T$, $U_Z$ are radial, tangential and vertical components of the particle velocity at the free surface, $i$ is the angle between the P rays and the vertical axis, and $j$ is the angle between the S ray and the vertical axis (Figure 1.1).

$$(U_R, U_T, U_Z) = \frac{\left[\frac{4\alpha p}{\beta^2}\frac{\cos i}{\alpha}\frac{\cos j}{\beta}, 0, \frac{-2\alpha}{\beta^2}\frac{\cos i}{\alpha}\left(\frac{1}{\beta^2} - 2p^2\right)\right]}{\left(\frac{1}{\beta^2} - 2p^2\right)^2 + 4p^2\frac{\cos i}{\alpha}\frac{\cos j}{\beta}}$$

Equation (1)

$$U_R, U_T, U_Z) = \frac{[\frac{2}{\beta}\frac{\cos j}{\beta}(\frac{1}{\beta^2} - 2p^2), 0, \frac{4p}{\beta}\frac{\cos i}{\alpha}\frac{\cos j}{\beta}]}{(\frac{1}{\beta^2} - 2p^2)^2 + 4p^2\frac{\cos i}{\alpha}\frac{\cos j}{\beta}}$$

Equation (2)

Then from equation (1), it is straightforward to obtain the ratio between the radial and vertical components of P waves,

$$\frac{U_R}{U_Z} = \frac{-2\beta p \cos j}{1 - 2p^2\beta^2}$$

Equation (3)

And similarly for the S wave,

$$\frac{U_Z}{U_R} = \frac{-2\beta p \cos i \quad \beta/\alpha}{1 - 2p^2\beta^2}$$

Equation (4)

For the incoming P wave, the ratio of radial to vertical component of particle motion (as displayed in equation 3) depends mostly on the shear velocity $\beta$ and ray parameter $p$ since $\cos j$ is close to one because of the small shear velocity near the free surface. From equation (4), it follows that Ps is much stronger on the radial component.

Since the ratio $\frac{U_R}{U_Z}$ of the P wave is proportional to the sub-surface shear velocity, this is then a good way to measure subsurface shear velocity when the ray parameter $p$ is known. Fortunately, the crustal structure in the CEUS is relatively simple (Ou and Herrmann, 1990). Therefore $p$ can be determined once the location and depth of an earthquake is well resolved, which is not an issue for events occurring inside the USARRAY.

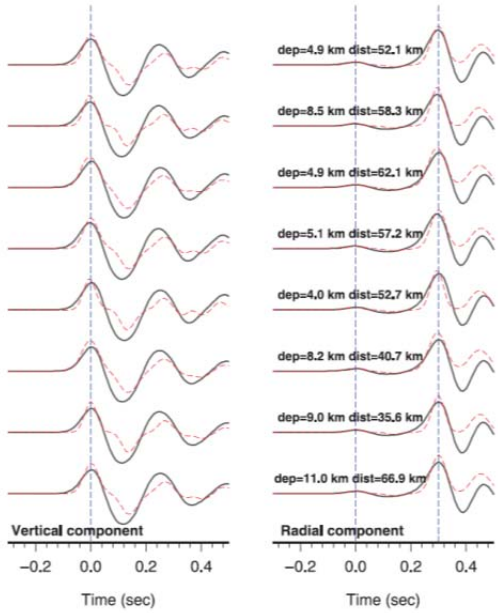


Figure 1.2. Comparisons of the waveforms computed by FK with explosion source (black lines) and plane wave synthetic seismograms (dashed lines). The focal depth and epicentral distance used in the FK computations are labeled above each radial waveform.

## 3. Numerical simulation of three-component P waves for different subsurface structures

In order to confirm that the ratio $\frac{U_R}{U_Z}$ of the P wave is mostly sensitive to subsurface shear velocity, we computed synthetic seismograms of three-component P waves. For 1D horizontally layered velocity models, two approaches can be taken for calculating synthetic waveforms. One approach is the wave number -frequency integral method which takes into account full waves for a point source with focal mechanism (Zhu and Rivera, 2002). This approach is time consuming when high frequencies (for example, 20Hz and above) are involved. The other approach assumes that the initial portion of P waves is generated by incident plane P waves, so an integral only in the frequency domain is required and computation is much faster (Randall, 1989). As displayed in Figure 1.2, synthetic seismograms from the two approaches agree well. Hereafter, we adopt the plane wave approximation for computing synthetic seismograms.

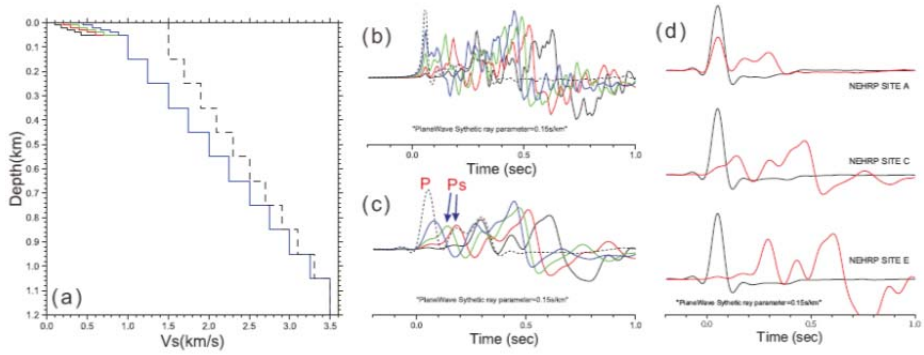


Figure 1.3. (A) Five shear wave velocity models corresponding to NEHRP A (dashed black), B (blue), C (green), D (red) and E (solid black) site classes. (B) Corresponding synthetic seismograms of radial components of local P waves, assuming a source time duration 0.05 second. (C) Same as (B), but source time duration is 0.1second. (D) Comparison of radial (red) and vertical (black) component of local P waves for NEHRP sites A (top), C (middle) and E (bottom). On the radial component, the direct P wave is smaller and secondary arrivals are much stronger when the sub-surface shear velocity is smaller.

To demonstrate that the radial and vertical ratio of the P wave is sensitive to subsurface shear velocity structure, we compute synthetic seismograms for five velocity models, in which the top 30m shear velocity (Vs30) corresponds to the five NEHRP site classes (A, B, C, D, E) respectively (Figure 1.3A). In Figure 1.3B, the radial component for each subsurface model is displayed, and the source duration is chosen to be very short (0.05 second) so that individual seismic phases are isolated from each other. It is obvious that for the radial component of synthetic seismograms, smaller subsurface shear velocity is always associated with smaller P amplitude and larger amplitude of secondary arrivals, which could consist of Ps and its multiples. When the source time function is chosen to be 0.1 second (appropriate for M3 earthquakes), a similar pattern can be observed in Figure 1.3(C) as in Figure 1.3(B). In both Figure 1.3(B) and Figure 1.3(C), the NEHRP site class A model shows the strongest P amplitude and the smallest secondary arrivals on the radial component. Although the subsurface shear velocity models affect the radial component of P waves, the vertical component (black traces) is not affected much (Figure 1.3D). From this figure, it is clear that the ratio $\frac{U_R}{U_Z}$ of the P wave is indeed very sensitive to subsurface velocity. For NEHRP sites C and E, the stronger secondary arrivals lag the

direct P wave by 0.15 second and 0.3 second respectively. Such a lag can be readily observed on broadband or short period seismograms with sampling rate of 20 samples per second or higher.

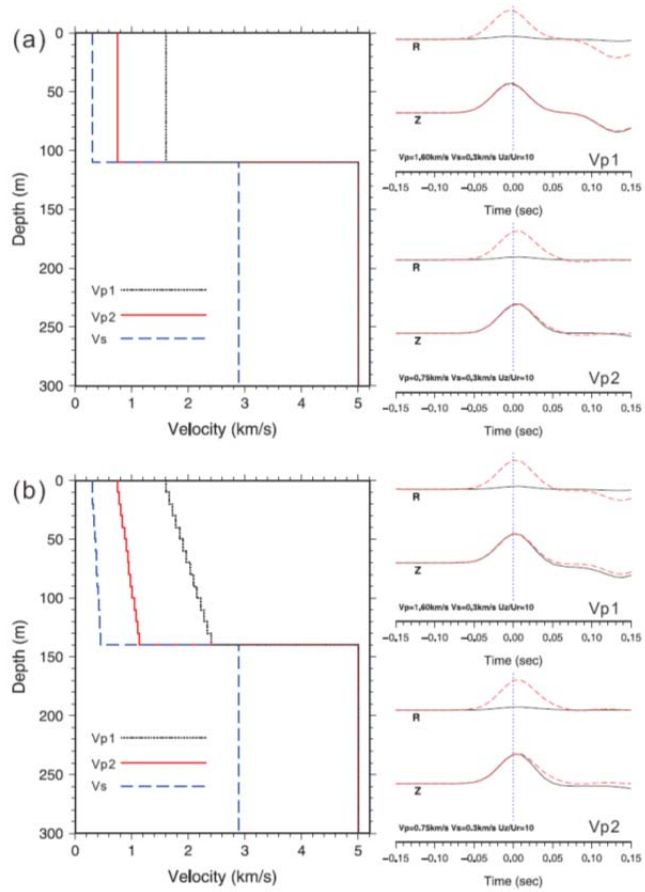


Figure 1.4. Tests of the sensitivity of the ratio Uz/Ur to the P-wave velocity within (a) constant velocity (b) linear gradient velocity layers. The waveforms shown in the right column are calculated with plane wave approximations. Solid and dashed lines indicate the vertical and radial components of seismic waveforms, respectively. For each sub-panel of seismograms, the amplitude of the radial component is plotted with same scale in the top trace, but is enlarged 10 times in the bottom trace to facilitate comparison.

We also test whether the radial component of the P wave depends on the subsurface P wave velocity. In Figure 1.4(a), a 100m layer with shear velocity of 300m/s situated on a half space and two P velocity models are tested (Vp of 0.75km/s and 1.6km/s respectively). Synthetic seismograms for the two P velocity models are almost identical, indicating that sub-surface P velocity does not affect the radial component of initial P waves. Synthetic seismograms for the

models with a top layer with linear velocity gradient (Figure 1.4b) again confirm that the radial component of the initial P wave is not sensitive to subsurface P velocity.

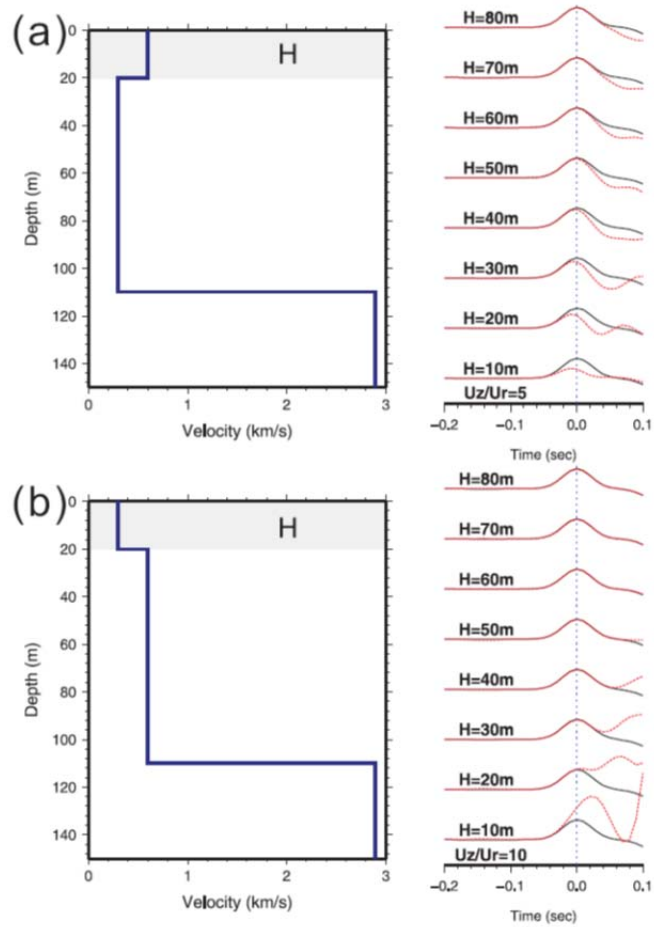


Figure 1.5. Synthetic waveforms calculated from two models with high (a) and low (b) subsurface shear-wave velocity layer. In the right column, solid and dashed lines indicate the vertical and radial components of seismic waveforms, respectively. Note that the amplitudes of radial components are enlarged 5 times for the top panel and 10 times for the bottom panel. The thickness and the shear-wave velocity of the uppermost layer are labeled above each trace.

As the ratio of radial and vertical initial P waves has to be measured over a finite time window, the inferred subsurface shear velocity is not necessarily the shear velocity for zero depth. Instead, the inferred shear velocity should represent the average from the surface to some depth. Usually the resolving capability of seismic body waves is limited by wavelength. Therefore, the inferred subsurface shear velocity could be the averaged velocity for the depth range of one wavelength of the S wave. In Figure 1.5a and 1.5b, we display synthetic

seismograms for velocity profiles consisting of a top layer of fast velocity (Vs = 0.6km/s) and low velocity (Vs=0.3km/s) respectively. The thickness of the top layer varies from 10m to 80m with increments of 10m. The earthquake source time function is set to be a 0.1sec wide pulse (typical for M3 earthquakes). From the synthetic seismograms, it is observed that only when the layer thickness is larger than the wavelength of S waves (0.1 sec times the shear velocity), does the radial component of initial P waves have the same waveform as the vertical component and show the expected amplitude. That is to say, the depth extent resolvable from the ratio of radial to vertical P wave amplitudes depends on the earthquake source duration.

**4. Observed three component P waves from local earthquakes and validation with measured shear wave velocity profiles**

An observation from the April 18, 2008 Mt Carmel earthquake sequence is displayed in Figure 1.6 for the ANSS station OLIL. For each aftershock, a clear P wave can be observed and the radial component of the P wave is much weaker than the vertical component for the first 0.2 second. Moreover, on the radial component there are strong secondary arrivals after the direct P wave, with features similar to those in Figure 1.3 for the case of NEHRP site class C.

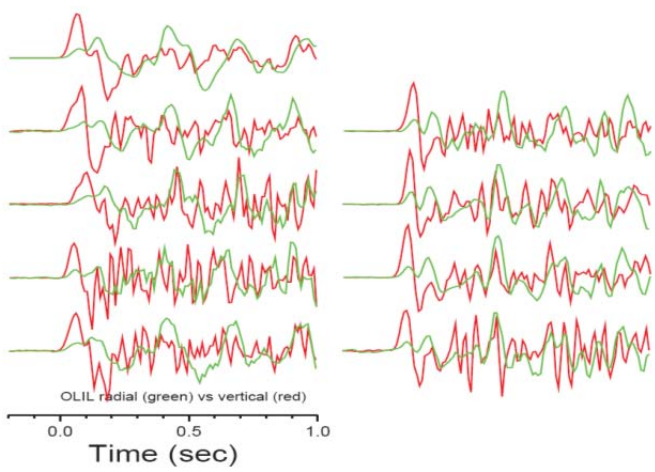


Figure 1.6. Radial (green) and vertical (red) component of P waves recorded at station OLIL from an aftershock of the 2008 Mt Carmel earthquake.

Odum et al (2010) performed detailed studies of five ANSS stations in the CEUS, and found that Vs30 is 480m/s for station OLIL from the ReMi technique. We take the subsurface velocity model from their ReMi result and compute synthetic seismograms of P waves. The synthetic seismograms (Figure 1.7) explain major features on the observed P waveforms as displayed in Figure 1.6, with smaller P amplitude on the radial component, Ps lagging P by 0.1 second, and a

fairly strong arrival about 0.5 second after the P wave. Hence, the initial few tenths of a second of three component P waveforms have enough resolving power to estimate subsurface shear velocity profiles.

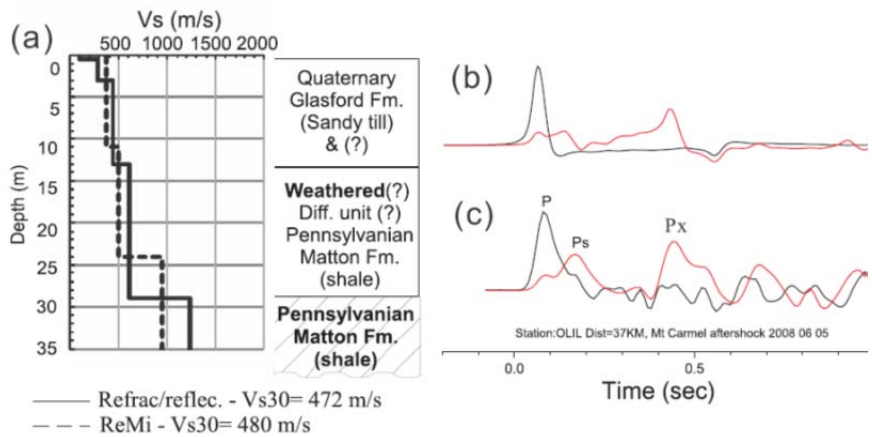


Figure 1.7. (a) Shear velocity model for station OLIL, determined with ReMi (dashed), adopted from Odum et al (2010). (b) Synthetic radial (red) and vertical (black) components of P waves. (c) Observed radial (red) and vertical (black) component of P waves recorded at station OLIL from an aftershock of the 2008 Mt. Carmel earthquake.

The waveforms of the radial components (red) in Figure 1.6 show some variability, and this could be related to the different waveforms of the vertical components (green). In a way analogous to teleseismic receiver functions, we can compute a local receiver function by deconvolving the radial component from the vertical component. The deconvolution is performed with an iterative deconvolution procedure in the time domain (Ligorria and Ammon, 1999), and the results are displayed in Figure 1.8a. The deconvolved waveforms are very similar for different events, showing that the initial portion of P waves is mostly sensitive to structure beneath the receivers, and not very sensitive to the location and depth of the events.

The approach of deconvolving the radial component from the vertical component is necessary when waveform data of larger earthquakes are used to study sub-surface structure, because the source function time could be much longer than the time window (typically less than 1 second) useful for sub-surface studies. For example, the local receiver function of the Mw 5.2 2008 Mt. Carmel main shock (red trace in Figure 1.8B) is very similar to those of the aftershocks (black traces), demonstrating the feasibility of modeling sub-surface structure with waveform data from

earthquakes up to M5. There are subtle differences between the red and black traces that may be caused by source complexities or differences in location and depth.

As mentioned above, the vertical P waveform is not much modified by subsurface structure. Therefore resolving subsurface structure from local waveforms is very similar to resolving crustal structure with teleseismic P receiver functions (Langston, 1989; Ligorria and Ammon, 1999), where it is assumed that vertical P wave propagation is simple. The major difference between resolving subsurface velocity structure and resolving crustal structure is temporal precision. Teleseismic P waves are only capable of providing robust planar P waves with frequencies below 2Hz (due to mantle attenuation and scattering of 3D crustal heterogeneity). In contrast, subsurface velocity structure can be resolved at frequencies as high as 10 Hz (for M3 events) or 20 Hz (for M2 events). Also, 3D crustal heterogeneity is less of a problem because only tens of meters to hundreds of meters in the region near the site are involved.

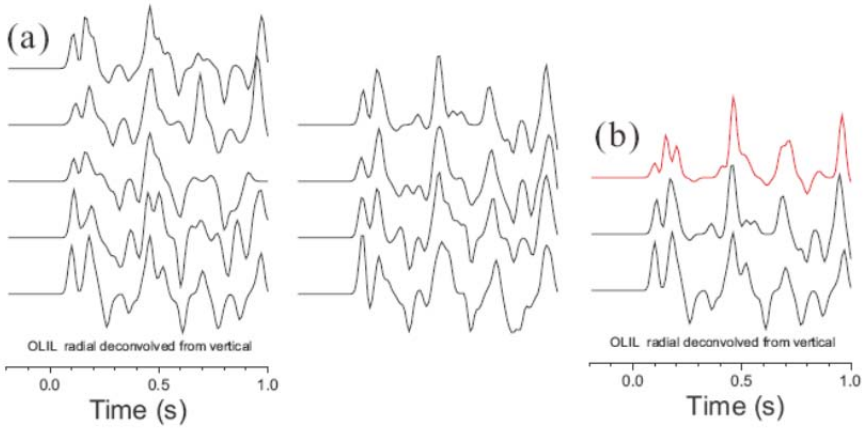


Figure 1.8 (a) Local receiver functions obtained by deconvolving the radial component from the vertical component of P waves recorded at station OLIL for aftershocks of the 2008 Mt Carmel earthquake which are displayed in Figure 1.6. (b) Comparison of local receiver functions at station OLIL for the main shock (red) and some aftershocks (black) from the 2008 Mt Carmel earthquake.

Consequently, algorithms used for resolving subsurface velocity structure with the initial portion of the local P wave can be the same as those used in teleseismic P receiver functions. Among many inversion schemes, global optimization methods such as the Neighborhood Algorithm (NA) and the Differential Evolution (DE) method have the advantage of finding the global minimum, and are particularly appropriate for highly nonlinear problems such as P receiver functions (Li et al, 2010; Sambridge 1999a, b). We adopt the technique used by Li et

al (2010), who obtained a high quality crustal model at station BJT in China using teleseismic P receiver functions. To demonstrate that the DE inversion algorithm is effective for inverting shallow velocity structure, we apply the algorithm to local receiver functions recorded at station OLIL. After 1000 iterations, a minimum in misfit between observed and predicted local receiver functions is achieved (Figure 1.9). Overall, the shear velocity model for the top 60 meters agrees with those measured from ReMi and Refrac/refl methods (Figure 1.9(d)).

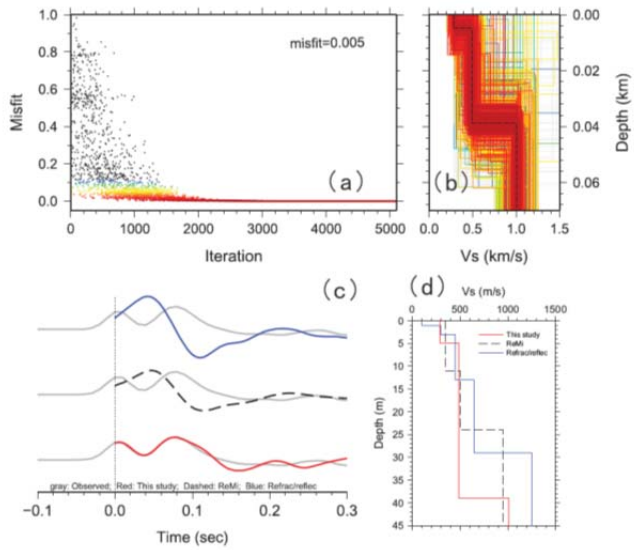


Figure 1.9. An example of applying the DE method for inversion of crustal structure beneath the OLIL station. (a) Evolution of misfit between observation and prediction of receiver function as a function of iteration. After 1000 iterations, minimal misfit is achieved. (b) The preferred model (dashed line) and suite of candidate models. (c) Observed (black) and synthetic receiver functions for three models (blue for Refrac/Reflect model, dashed for ReMi model and red for model inverted from this study. (d) Comparison between preferred model and the models from Refrac/Reflect and ReMi methods.

**Part II**

# Application of initial local P waves to resolve shallow shear-wave velocity structure beneath Station CBN for the $M_w$ 5.8 Mineral, Virginia earthquake sequence

## 1. Introduction

On 23 August 2011, a $M_w$ 5.8 earthquake occurred in Virginia, United States (referred as the Mineral earthquake hereafter) (Fig. 2.1), which is the largest earthquake in the Central and Eastern United States (CEUS) in the last 100 years. The Mineral earthquake caused light to moderate damage in the surrounding regions, including central Virginia and Washington D.C. Tens of $M$ 2 or larger aftershocks occurred around the Mineral earthquake (Fig. 2.1). In view of the low seismic activity in the CEUS, this earthquake sequence provides a valuable dataset for modeling ground motion prediction equations. However, the USARRAY has not covered the epicentral region yet and only a few permanent seismic stations recorded the Mineral earthquake sequence within an epicentral distance of 100km. Among these stations, CBN of the USNSN network is the closest permanent backbone station of ANSS, and about 58 km away from the Mineral earthquake (Figure 2.1). Although CBN is not the closest station (the non-backbone CVVA station is the closest station with an epicentral distance about 54 km), it recorded the maximum peak ground velocity (PGA) of 0.135 g, which is ~11% larger than the PGA of 0.121 g at CVVA (referred to http://www.strongmotioncenter.org/). Stronger ground motion at a more distant station could possibly be attributed to a difference in site response.

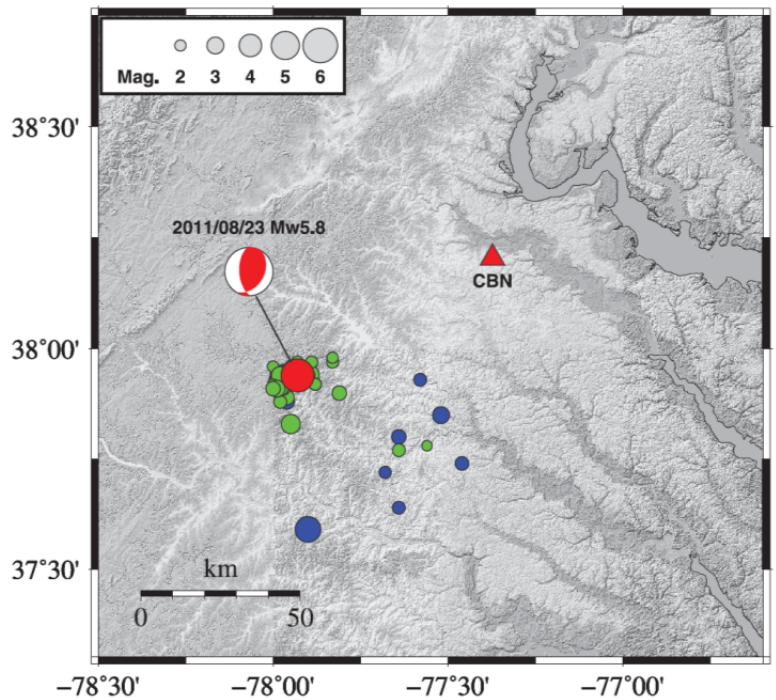


Figure 2.1. Topographic map of the region around the $M_w$ 5.8 Mineral earthquake on 23 August 2011 (red circle). Triangle shows the location of station CBN. Circles indicate the earthquakes from 2001 to 2012. Blue and green circles show the earthquakes before and after the occurrence of the Mineral earthquake, respectively. Note that the epicentral distances to CBN for the earthquakes are all within 100 km.

As one of the major components of ground motion prediction equations, site characterization is essential for seismic hazard analysis. Site response is mostly controlled by the subsurface shear-wave velocity structure, especially the top tens to hundreds of meters (Boore, 2006; Wald and Mori, 2000). The average shear-wave velocity of the top 30 m ($V_s30$) is an important parameter for classifying earthquake site response (Boore, 2004). However, shear-wave velocity structure down to hundreds of meters is also necessary when assessing site response. At a minimum, the shear-wave velocity structure of the unconsolidated sediments with thickness from tens to hundreds of meters or more, which usually has very low shear-wave velocity (down to ~ 100 m/s) (Chiu and Langston, 2011), should be thoroughly studied. Therefore, in order to better evaluate site response for strong ground motion simulation of the Mineral earthquake, it is necessary to study the subsurface shear wave velocity structure in the surrounding region. As station CBN recorded the strongest ground motion among backbone

ANSS stations, it is necessary to understand the site response beneath that station to infer the ground motions that would have been recorded for rock site conditions.

Table 2.1. Crustal Velocity model (CEUS) beneath the sediment layer (http://www.eas.slu.edu/eqc/eqc_mt/MECH.NA/20110823175105/index.html).

| Thickness(km) | *Vp* (km/s) | *Vs* (km/s) |
|---|---|---|
| 1 | 5.00 | 2.89 |
| 9 | 6.10 | 3.52 |
| 10 | 6.40 | 3.70 |

## 2. Methodology

A detailed review of both active and passive methods for determining subsurface velocity structure was made by Boore (2006). Proxy methods such as slope, terrain and mapped surface geology have also been proposed for characterizing site effects (Wald and Allen, 2007; Yong et al., 2012; Kottke et al., 2012). In this report, we use a newly developed method to study the shallow shear-wave velocity structure with three-component local earthquake *P* waves. From the theoretical derivation in Part I, it has been demonstrated that the amplitude ratio of radial to vertical initial *P* waves is a good indicator of subsurface shear-wave velocity. The shear-wave velocity of the uppermost surface can be represented as equation (3) in part I, which shows that the amplitude ratio of radial to vertical *P* waves depends mostly on the shear velocity $\beta$ and ray parameter $p$. This approach has been validated for ANSS stations in the central and eastern US, and it is found that the method outperforms the other methods (Kim et al., 2013). Moreover, for the case of unconsolidated sediment overlying hard rock, the incoming *P* wave can be converted to an *S* wave named *Ps* (Langston, 2003a) due to the sharp contrast between sediment and bedrock. When the source duration of a local earthquake is short enough (which is usually the case for small to moderate earthquakes), the direct *P* wave and the *Ps* wave can be observed as isolated pulses on the radial component. The amplitude of *Ps* and its time lag after the *P* wave provide extra constraints on the shear-wave velocity of the top layer of sediment. For example, the thickness of unconsolidated sediments in the Mississippi embayment is resolved by modeling the timing and strength of Ps from local earthquakes (Chiu and Langston, 2009, 2011), and attenuation parameters can even be estimated by modeling the direct and converted phases (Langston, 2003b).

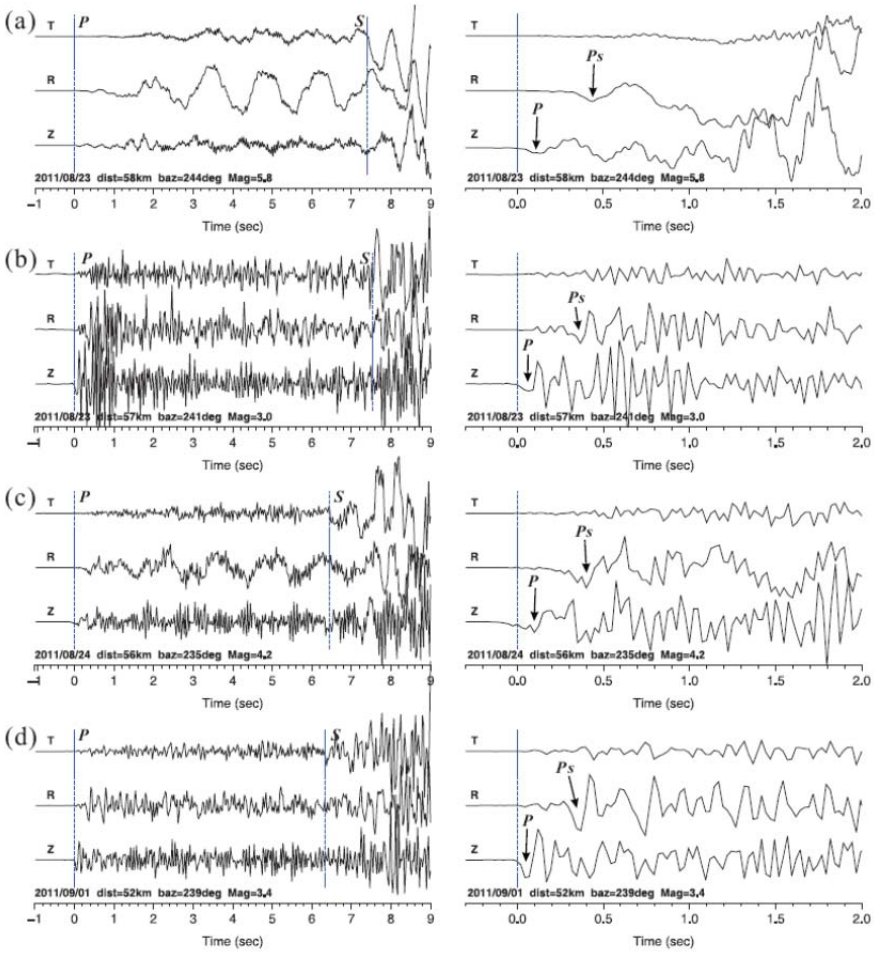


Figure 2.2. Waveforms of (a) mainshock and (b-d) aftershocks of the Mineral earthquake at CBN. Left column: Strong oscillatory waveforms between first *P* and *S* arrivals. Right column: Clear *Ps* phases with ~0.3 s delay. First *P* and *S* arrivals are labeled on each waveform. The origin time, epicentral distance and magnitude of each earthquake are labeled on the lower left corner of each figure. The flat tangential waveform around ~0.5 s after the first *P* arrival indicates that the three-component waveforms are rotated into Z, R and T directions.

## 3. Data

Table 2.2. Parameters of earthquakes used in this study.

| Origin Time | | Location | | Depth | Magnitude | Distance |
|---|---|---|---|---|---|---|
| year/month/day | hr:min:sec | (°N) | (°W) | (km) | | (km) |
| 2009/07/07 | 03:59:52 | 37.64 | 77.64 | 11.0 | 2.3 | 67 |
| 2009/08/02 | 21:57:07 | 37.93 | 77.58 | 9.0 | 2.3 | 36 |
| 2010/10/02 | 20:17:00 | 37.84 | 77.42 | 8.2 | 2.9 | 41 |

| | | | | | | |
|---|---|---|---|---|---|---|
| 2010/10/30 | 06:10:13 | 37.74 | 77.46 | 4.0 | 2.4 | 53 |
| 2011/08/23 | 18:46:49 | 37.95 | 77.94 | 5.1 | 3.0 | 57 |
| 2011/08/24 | 04:45:26 | 37.93 | 77.99 | 4.9 | 3.4 | 62 |
| 2011/08/30 | 03:48:28 | 37.93 | 77.94 | 8.5 | 2.5 | 58 |
| 2011/09/01 | 09:09:37 | 37.96 | 77.88 | 4.9 | 3.4 | 52 |

Station CBN is equipped with both broadband seismometers and accelerographs. At epicentral distances of around 60km, high quality waveform data have been recorded at CBN from tens of local earthquakes including the Mineral earthquake and its aftershocks. We collected the seismic waveforms at CBN from local earthquakes that occurred between January 2001 to June 2012 (Figure 2.1, Table 2.2). As displayed in Figure 2.2, direct *P* and *S* waves are clearly observed on these local waveforms (*M*2-*M*4 for aftershocks)., The first pulse of the *P* waves on the radial component are much weaker than those on the vertical component, suggesting that the subsurface shear velocity (Vs) is very low (from equation 3, the lower the Vs, the weaker the P wave on radial component). Moreover, as shown in Figure 2.3, there are strong secondary arrivals about 0.3 second after the *P* wave on the radial component. Good coherence of the radial and the vertical waveforms can be achieved with a time shift of ~0.3 s on the radial component. Their almost identical waveforms suggest that the strong secondary arrival on the radial component is converted from the P wave at a sharp interface. We propose that the strong secondary arrival is the *Ps* wave from the boundary between unconsolidated sediments and hard bedrock, because similar features are observed in the Mississippi embayment (Langston, 2003a).

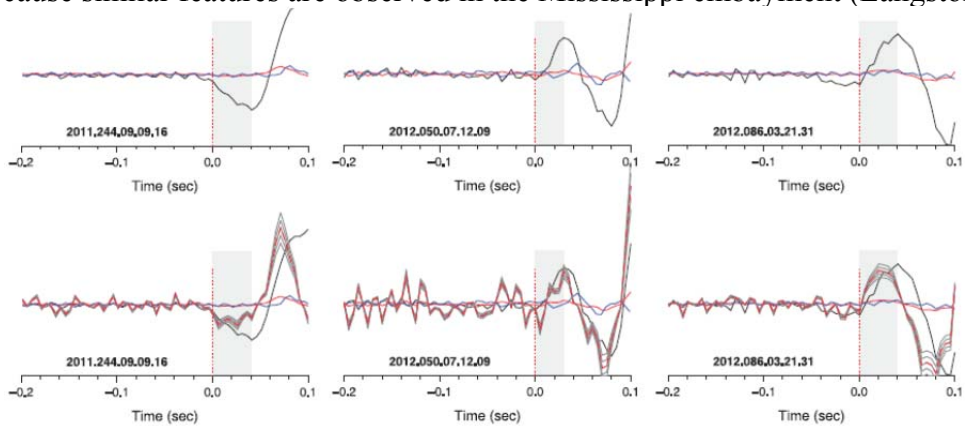


Figure 2.3. Vertical, radial and tangential component waveforms of 2011/09/01 *M*3.4 (left column) 2012/02/19 *M*2.7 (middle column) and 2012/03/26 *M*3.1 (right column) aftershocks of the 2011/08/23 Mineral earthquake. Upper row shows the original vertical (black), radial (red) and tangential (blue) component waveforms, while lower row shows the radial waveforms amplified by factors of 7, 8, 9, 11, 12, 13 (gray) and 10 (dashed red). The Uz/Ur approximately equals 10. The gray bars show the approximate time period from first arrival to the maximum amplitude of the *P* wave. The waveform are extracted from the high sample rate (200 sps), high gain data streams.

To resolve the subsurface shear velocity and depth of the sharp interface, we compute synthetic seismograms and compare them with observed waveform data. Synthetic displacement waveforms can be calculated by double integration in the frequency-wavenumber domain (FK) (Zhu and Rivera, 2002) or by single integration in the frequency domain by the reflection matrix approach using a plane wave approximation (plane wave method) (Haskell, 1960; Kennett, 1983; Randall, 1989). The latter assumes that seismic waves arrive with single slowness, and the single integral is much faster than the FK computation. As confirmed by Ni et al. (2013), the first 1-second segments of the P waveforms calculated using the plane wave approximation are consistent with those from the FK method for epicentral distances of several tens of kilometers. Thus, due to its computational efficiency, we adopt the plane wave method in computing the synthetic seismograms.

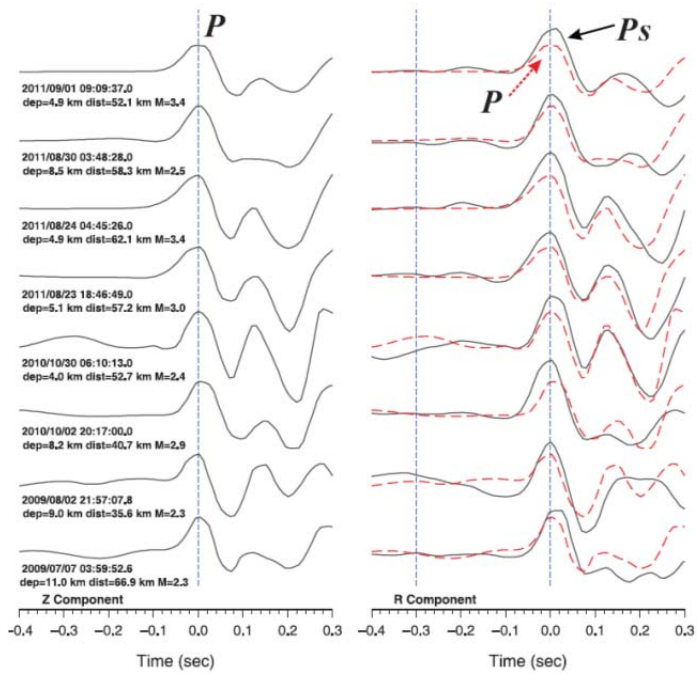


Figure 2.4. Good coherence between the vertical (left column) and the radial (right column) waveforms with a lag time of 0.3 s, suggesting that the radial components are converted from the *P* wave on the vertical components (*Ps*). Solid lines show the vertical (left column) and radial (right column) waveforms. Dashed lines on the right column show the vertical waveforms.

## 4. Analysis of the subsurface shear velocity and depth of the sediment-bedrock interface

From equation 1, we determine the shear-wave velocity of the uppermost surface at CBN by using the radial/vertical amplitude ratio (*Uz*/*Ur*) of the initial *P* waves (Figure 2.4). The broadband seismic waveforms (channel BHZ, BHN and BHE) of the CBN recording are digitized at 40 samples per second (sps), which is not sufficient for higher temporal resolution of the *Uz*/*Ur* ratio of the *P* wave. In order to estimate the shear-wave velocity of the surface sediments, we made the measurement on the *P* waves from the broadband, high sample rate (200 sps) component data stream (channel HNZ, HN1 and HN2). The *Uz*/*Ur* ratio of the *P* wave is measured by visual inspection, comparing the first wiggle of the P wave on the radial component magnified by factors from 5 to 20 with the first wiggle of the P wave on the vertical component. The slowness of the P wave (*p* in equation 1) is computed from the 1D CEUS crustal model assuming the hypocenter local and focal depth of Chapman (2013), and is found to be approximately 0.15 s/km. As shown in Figure 2.4, the *Uz*/*Ur* ratios of the *P* wave from three aftershocks are approximately 10, which, together with the measurements of another three aftershocks (not shown in the figure), indicate that the average shear-wave velocity at the uppermost surface (Vs) varies from 260 to 380 m/s with an average value of ~300 m/s (from equation 1). The source durations of the three local earthquakes are 0.1 s or less, suggesting the depth extent of this layer is ~30 m or less according to the equation for depth estimation assuming 0.1 sec × Vs ( as discussed in Part I).

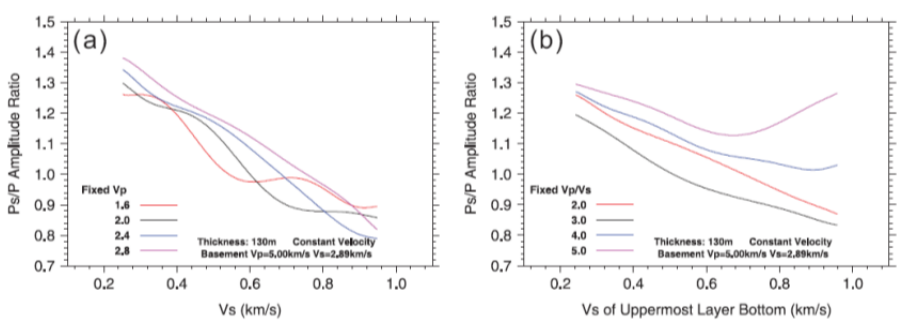


Figure 2.5. Variations of *Ps/P* from varying the uppermost shear-wave velocity with fixed *Vp* (a and c) and fixed *Vp*/*Vs* (b and d). Models with constant (a, b) and linear gradient (c, d) velocity layers are used in the plane wave computations. The uppermost shear-wave velocity is set to 300 m/s for (c) and (d). Model information is labeled on the bottom of each panel. The figure suggests that *Ps*/*P* could indicate the impedance contrast between the sediment and bedrock, but *Ps*/*P* varies slowly when the bottom shear-wave velocity varies between 200~500 m/s.

Assuming that the average shear-wave velocity of the whole sediment layer is ~300 m/s as an approximate estimate, the interval between the P and Ps wave can be used to estimate the sediment thickness. The waveform shapes and the amplitude ratio of *Ps* (*P*/*Ps*) provide further constraints on the thickness and the shear-wave velocity contrast across an interface when the bedrock model is known (Chen et al, 1996; Langston, 2003a; Chiu and Langston, 2011). The velocity model used in the moment tensor solution of SLU (hereafter referred as Model-CUS) (http://www.eas.slu.edu/eqc/eqc_mt/MECH.NA/20110823175105/index.html) is adopted as a reference model for bedrock beneath the unconsolidated sediment at CBN (Table 2.1). Moreover, the P velocity structure of the sediments is also a factor in the waveform modeling processes, and there are two approaches for P velocity parameterization. Langston (2003) found that *Vp* is around 2.0 km/s for the shallow unconsolidated sediments and that the *Vp*/*Vs* ratio can be up to 5. To test the effects of *P* velocity on waveform modeling, we designed two sets of *P* models, one model featuring homogeneous *Vp* in the top layer and the other with homogeneous *Vp*/*Vs* (Figure 2.5). The shear-wave velocity near the free surface is set to 300 m/s according to the measurement of the *Uz*/*Ur* ratio of the *P* wave described above. The average *Vp*/*Vs* of the unconsolidated sediments is set to 2 - 5 according to previous studies (Langston, 2003a; Brocher, 2008; Liu et al., 2011). Two shear velocity models (one with homogeneous velocity and the other with a linear gradient in the top layer) are used in the computation (Figures 2.5 and 2.6). For the models in Figure 2.5, the *P*/*Ps* amplitude ratio varies in the range of 1.1-1.5 (Figure 2.5), suggesting that the *P*/*Ps* amplitude ratios do not vary rapidly when the shear-wave velocity at the base of the sediments varies in the range of 200~500 m/s. Although definitive results are difficult to achieve due to the uncertainties in constraints on *Vp*, *Vp*/*Vs* and density, the *P*/*Ps* amplitude ratios can still provide constraints on the impedance contrasts of the interface beneath the unconsolidated sediment and the basement.

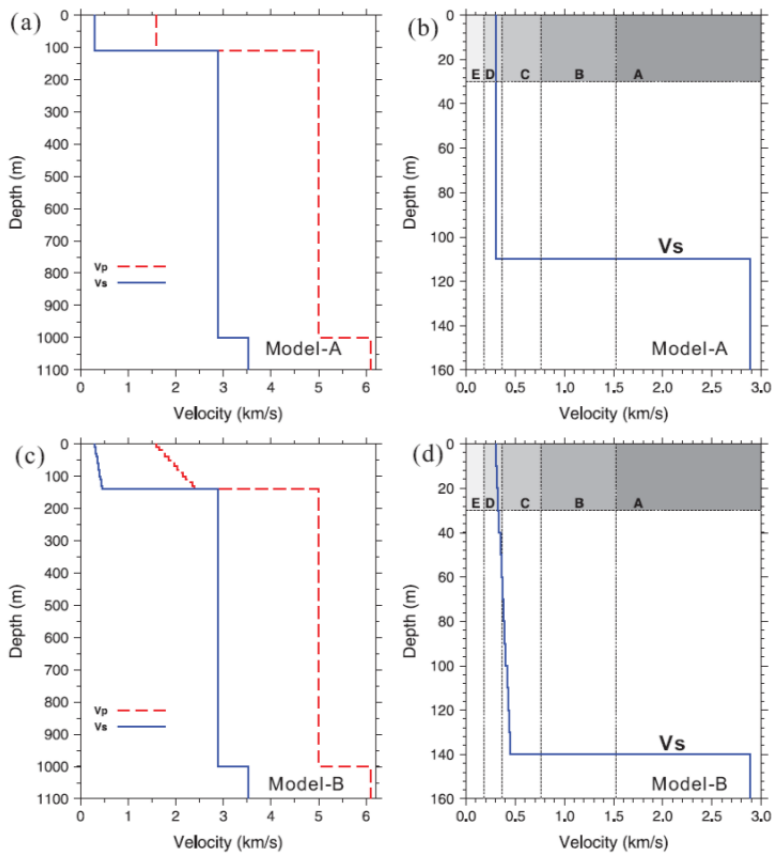


Figure 2.6. Two preferred velocity models at CBN. Upper row shows Model-A with constant velocity layer down to 110 m, while the lower row shows Model-B with linear gradient velocity layers down to 140 m. The shear- and compressional-velocities beneath the sediment are derived from the reference model for central United States (http://www.eas.slu.edu/eqc/eqc_mt/MECH.NA/20110823175105/index.html). The NEHRP site classifications are labeled in the right column based on the averaged shear-wave velocity in the top 30 m, indicating that the site classification at CBN is *D*.

We tested several models with different thickness and shear wave velocity at the base of the sediments, and finally proposed two models with different velocity structures to fit the waveforms of local earthquakes with epicentral distances of 36~67 km (Table 2.3) (Figure 2.6). Model-A features a homogeneous velocity layer down to 110 m, and Model-B features a linear gradient velocity layer down to 140 m. Both models can generally fit the observed waveforms (Figure 2.7). The arrival time difference between *P* and *Ps* is ~ 0.30 s, and the *P*/*Ps* amplitude ratio varies from 1.13 to 1.73.

## 5. Discussion and Conclusions

Local earthquake waveforms have demonstrated the potential for estimating the shallow shear-wave velocity structure in many studies. For example, the waveforms and arrival times of *P*- and *S*-wave reverberations (e.g., *Ps*, *Sp*, *PpPhp*) within the sedimentary column provide useful information on the velocity structure (Kruger, 1994; Chen et al. 1996; Langston 2003a, 2003b; Chiu and Langston 2009, 2011). However, the trade-offs between the layer parameters (e.g., layer thickness and velocity) in the study of velocity structure has also been well recognized (Langston 2003a, 2003b; Chiu and Langston, 2009, 2011).

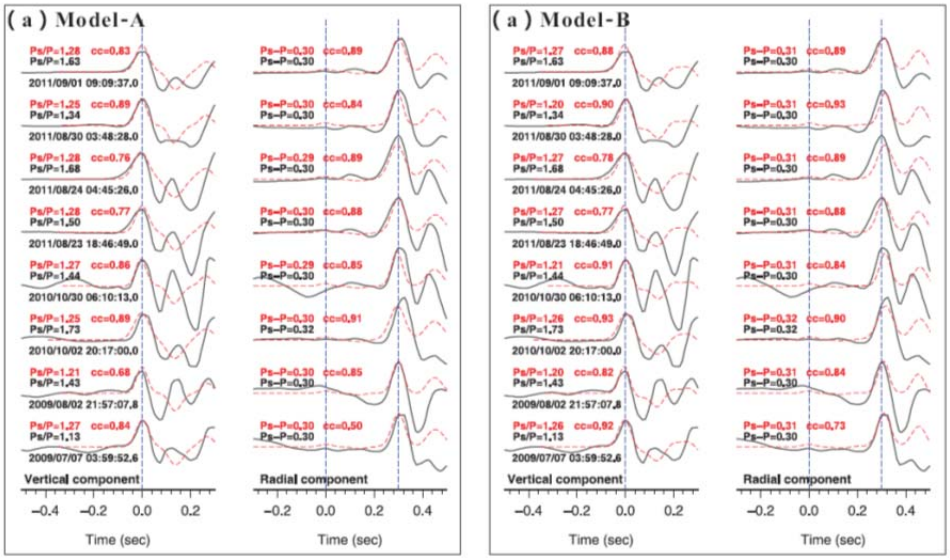


Figure 2.7. Waveform comparisons between observed (solid line) and synthetic waveforms (dashed line) from Model-A (a) and Model-B (b). Zero time indicates the maximum amplitude of the first *P* arrival.

The ratio *Uz*/*Ur* of the *P* wave used in this study provides estimates of the absolute shear-wave velocity of the uppermost surface if the ray parameter *p* is known (equation 3). The measurement of *Uz*/*Ur* and the estimate of the ray parameter *p* will affect the accuracy of shear-wave velocity estimates. When the shear-wave velocity becomes lower than 200 m/s, *Uz*/*Ur* is greater than ~15, suggesting that the amplitude of the *P* wave on the radial component is very small and noise on the radial component may hinder accurate measurement of *Uz*/*Ur*. Therefore, high SNR is needed for accurate *Uz*/*Ur* estimation. M3+ earthquakes recorded on local quiet stations are usually needed. The calculation of ray parameter could be affected by earthquake mislocation and bias in the crustal velocity model. However, for simple crustal structures such as those in the CEUS, the small variability of ray parameter for local earthquakes indicates negligible influence on the shear-wave velocity estimates. The source time function of earthquakes is another factor that will affect the measurement accuracy of *Uz*/*Ur*. The sensitivity of the depth extent of the surface layer to the average shear-wave velocity using the *Uz*/*Ur* ratio

is approximately proportional to the source duration time, i.e., the depth extent is in the range of source duration multiplied by the subsurface shear velocity (Langston, 2003a).

Table 2.3. Definition of NEHRP site classifications in terms of VS30 (FEMA, 2003).

| Site Class | Soil Profile Name | Average shear wave velocity in top 30 m (m/s), VS30 |
|---|---|---|
| A | Hard rock | VS30 > 1524 |
| B | Rock | 762 < VS30 ≤ 1524 |
| C | Very dense soil and soft rock | 366 < VS30 ≤ 762 |
| D | Stiff soil profile | 183 < VS30 ≤ 366 |
| E | Soft soil profile | VS30 < 183 |

Although uncertainties still exist in shear-wave velocity estimation, the estimated subsurface shear velocity still provides useful constraints on site characterization. For example, the NEHRP site classification using $V_{S30}$ is an important and widely used parameter for classifying sites and predicting their potential to amplify seismic shaking (Table 2.3) (Boore, 2004). Typically, if *Uz*/*Ur* of local P waveforms can be measured with an accuracy of 50%, then the subsurface shear velocity estimation is helpful for NEHRP site characterization.

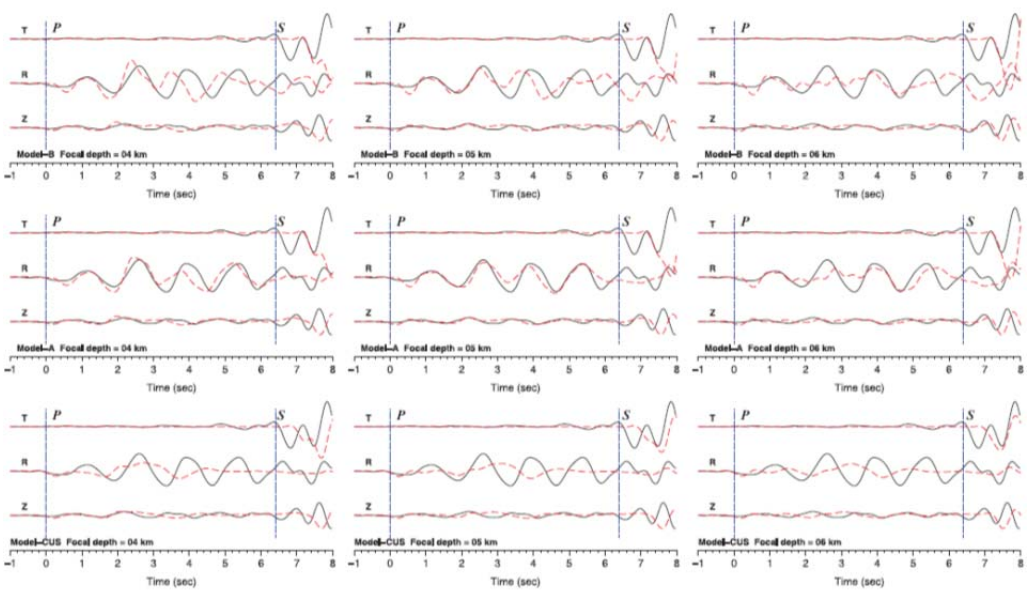


Figure 2.8. Synthetic (dashed line) and observed (solid line) waveforms of the Mineral earthquake at CBN. Synthetic waveform are calculated from Model-CUS, Model-A, and Model-B. Synthetic waveforms from Model-CUS show relatively simple waveforms between the first *P* and *S* arrivals, and cannot predict the oscillatory wiggles. In contrast, synthetic waveforms from both Model-A and Model-B have oscillatory wiggles like those in the observed waveforms between first *P* and *S* arrivals. The results suggest that shallow velocity structure is needed in the 1-D Model-CUS. Note that different focal depths (4 km for left, 5 km for middle and 6 km for right column) are used in the synthetic waveform calculation. A band pass filter of 0.05~2 Hz is used for all waveforms.

However, not only the shallow velocity structure in the upper 30 m ($V_{S30}$) of the sediment, but also the deeper structure could affect strong ground motion amplitudes. Therefore, the velocity structure of the entire unconsolidated sedimentary sequence needs to be investigated. Once the shear-wave velocity of the uppermost sediment is determined, the deeper velocity structure can be better resolved by the constraints of arrival time difference, *P*/*Ps* of *P* and *Ps* in local earthquake waveforms, which have shown their potential in velocity structure studies (Chen et al., 1996; Langston, 2003a, 2003b; Chiu and Langston, 2009, 2011).

With the improved models (Model-A and Model-B shown in Figure 2.6), we calculate the full waveforms of the Mineral earthquake at CBN station and compare them with the synthetic waveforms from Model-CUS (Fig. 2.8). Probably due to the ~100 m thick low shear-wave velocity layer in Model-A and Model-B, strong oscillatory wiggles on the radial component between the first *P* and *S* arrivals can be predicted much better than that from Model-CUS (Fig. 2.8), suggesting that a low shear-wave velocity layer atop the bedrock is required to explain the data. Not only the waveforms between *P* and *S* are better explained, the whole wave trains from Model-A and Model-B agree better with the observation than the Model-CUS, especially for the amplitude of the tangential component (Fig. 2.9). The maximum amplitude of the tangential waveforms from Model-A and Model-B is ~3 times of that from Model-CUS, suggesting that the shallow low shear-wave velocity layer should be carefully considered when simulating strong ground motion.

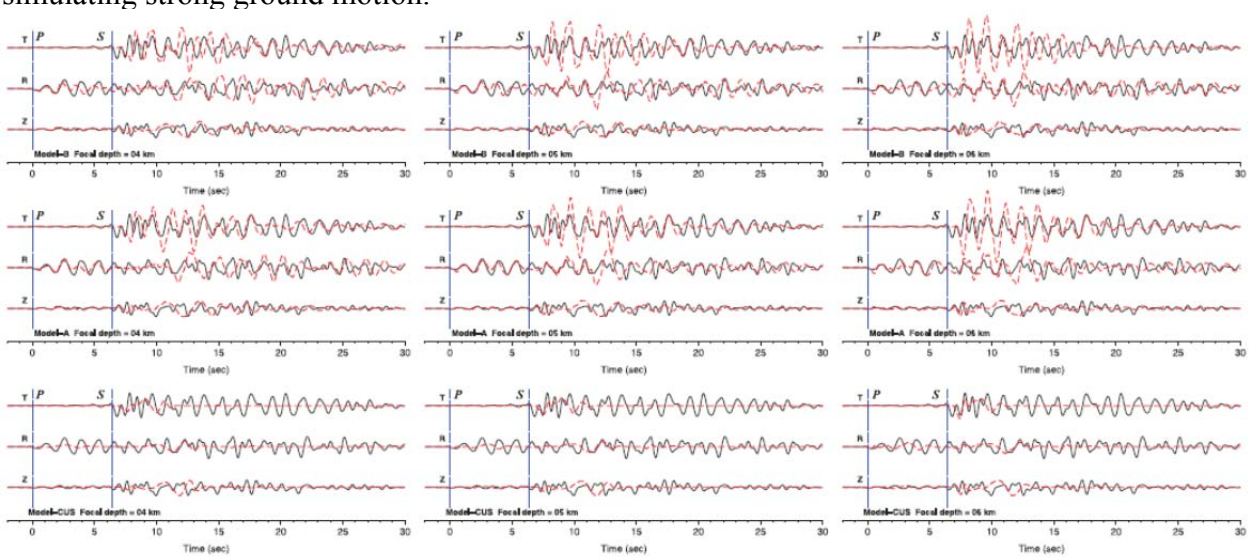


Figure 2.9. Synthetic (dashed line) and observed (solid line) waveforms of the Mineral earthquake at CBN. Synthetic waveforms are calculated from Model-CUS, Model-A, and Model-B. Synthetic waveforms from Model-CUS show relatively simple waveforms between the first *P* and *S* arrivals, and cannot predict the oscillatory wiggles. In contrast, synthetic waveforms from both Model-A and Model-B have oscillatory wiggles like those in the observed waveforms between the first *P* and *S* arrivals. The results suggest that shallow velocity structure is needed in the 1-D Model-CUS. Note that different focal depths (4 km for left, 5 km for middle and 6 km for right column) are used in the synthetic waveform calculation. A band pass filter of 0.05~2 Hz is used for all waveforms.

In conclusion, with local *P*-wave waveforms from the Mineral earthquake sequence and nearby earthquakes, an average shear-wave velocity (~ 300 m/s) in the top ~30 m at CBN is estimated by measuring the ratio of vertical/radial component of the *P* wave (*Uz*/*Ur*). The NEHRP site classification based on $V_{S30}$ is determined to be *D* (183 m/s < $V_{S30}$ ≤ 366 m/s). The shear-wave velocity structure of the entire unconsolidated sediment sequence at CBN is obtained by the constraints of *P* and *Ps* wave shapes, arrival time differences and *P*/*Ps* amplitude ratios using local earthquake waveforms. Two models, one with constant velocity (Model-A with a low shear-wave velocity layer of ~110 m thickness) and the other with a linear gradient (Model-B with a low shear-wave velocity layer of ~140 m thickness) both fit the observations well. Since site response is basically controlled by the subsurface shear velocity of the top tens to hundreds of meters, the proposed model can be used to investigate site response near the CBN. Moreover, by using the continuous waveforms recorded by the USARRAY and ANSS stations, the noninvasive, low-cost and single-station method used in this study is able to infer the shear-wave velocity structure and site response using the *P* waveforms from *M*2 - *M*4 local earthquakes in the CEUS.

## Part III
## Estimating Subsurface Shear Velocity for Stations in the Central and Eastern US (CEUS) with the Amplitude Ratio of Radial to Vertical Component of Local P waves

### 1. Measuring Ur/Uz with cross correlation method.

As prescribed by equation (3) in Part I and confirmed by detailed modeling of waveforms at station OLIL for the 2008 Mt. Carmel earthquake and waveforms at station CBN for the 2011 Mineral, Virginia earthquake, three component waveforms of initial local P indeed are capable of constraining subsurface shear velocity structure beneath seismic stations. However, for the 1000+ stations in the CEUS (including stations in EM,ET,IM,IU,LD,TA,US,XI,XR,Z9,ZL), it is challenging to perform detailed waveform modeling (e.g., waveform inversion of the local P receiver function) for each seismic station and each M2+ earthquake. Actually, even the measurement of Ur/Uz is time consuming given that there are many M2+ earthquakes in the CEUS and 1000+ stations. For example, with visual inspection, it takes many trials to measure Ur/Uz for station CBN (Figure 3.1, same as Figure 2.2), and there is some subjectivity in determining what the best measurement of Ur/Uz is. Therefore, an automatic procedure of measuring Ur/Uz is needed for processing the large numbers of waveforms.

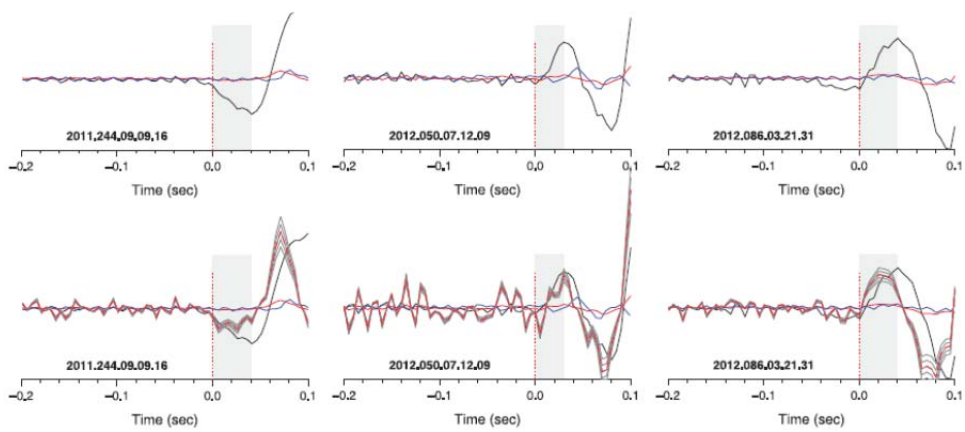


Figure 3.1. Vertical, radial and tangential component waveforms of 2011/09/01 *M*3.4 (left column) 2012/02/19 *M*2.7 (middle column) and 2012/03/26 *M*3.1 (right column) aftershocks of the 2011/08/23 Mineral earthquake. Upper row shows the original vertical (black), radial (red) and tangential (blue) component waveforms, while lower row shows the radial waveforms amplified by factors of 7, 8, 9, 11, 12, 13 (gray) and 10 (dashed red). The Uz/Ur approximately equals 10. The gray bars show the approximate time period from first arrival to the maximum amplitude of the *P* wave. The waveform are extracted from the high sample rate (200 sps), high gain data streams.

We adopt a cross-correlation algorithm for measuring Ur/Uz which basically simulates the visual inspection process. That is, Ur/Uz is chosen as the best coefficient of *x* by minimizing the difference between *R(t) – x Z(t)* for a short time window just after the onset of the P wave, where *R(t)* and *Z(t)* are the radial and vertical components of P respectively. It is straightforward to show that *x = R(t) * Z(t) / Z(t) *Z(t)*, where * is the cross-correlation operator defined as R(t)* Z(t) = $\int_0^T R(t)Z(t)dt$, T is the time window duration of P and 0 indicates the onset of P. In order to include the whole P wave pulse, T is chosen to be at least longer than first the swing of the P wave (that is, starting from onset of P to the first zero of P waves). For weak earthquakes (M<4) , high pass filtering is usually needed to enhance the signal noise ratio of P waves.

In order to assess the robustness of Ur/Uz measurement for different frequency bands and time window durations T,. we test high pass filters of 1Hz, 2Hz and 4Hz (because microseismic noise is weak for frequencies higher than 1 Hz,), and we also test the effects of T (0.2 sec, 0.4 sec, 0.6 sec and 0.8 sec) on measurement of Ur/Uz.

Seismograms of raw and high-pass filtered waveforms are displayed in Figure 3.2 for station Y44A of the USARRAY network. On the raw seismograms, long period noise (5sec or longer) is strong. With high-pass filtering at 1Hz, the noise before the P wave is substantially suppressed. For 2Hz and 4Hz high-pass filtering, the signal noise ratio (SNR) is further enhanced, but the P waveform becomes more complicated at higher frequencies. Figure 3.3 shows the same information for station X40A.

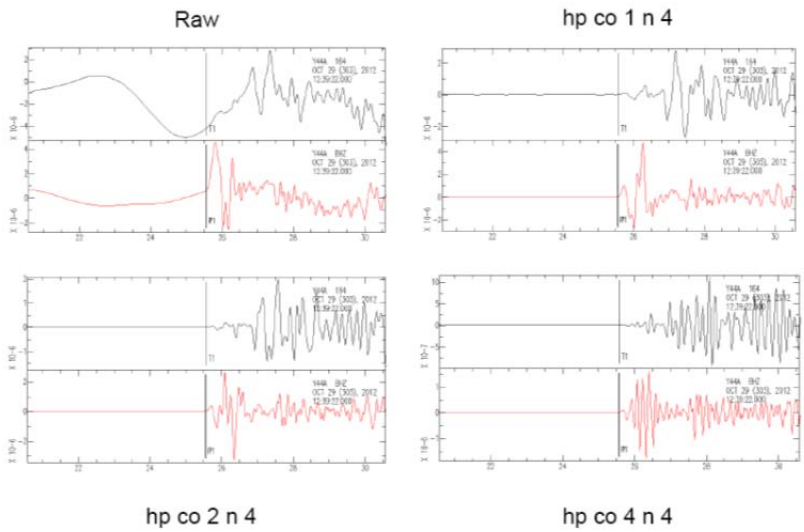


Figure 3.2. Raw (top left) and high-pass filtered seismograms at station Y44A(black: radial component and red: vertical component). 1Hz, 2Hz and 4Hz high-pass filters are applied for top right, bottom left and bottom right panels respectively.

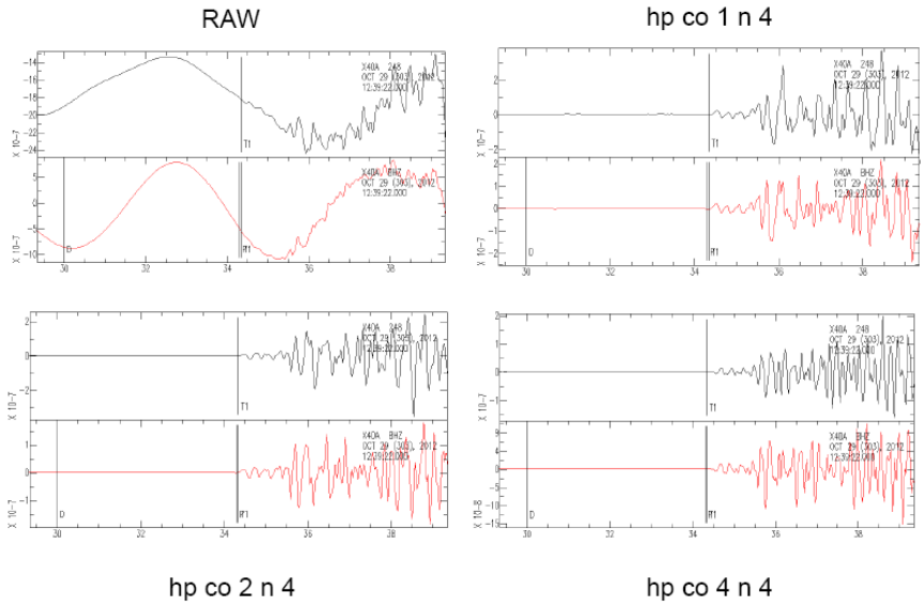


Figure 3.3.Same for Figure 3.2, but for station X40A.

Ur/Uz is measured for different filter parameters and time durationsT as displayed in Figures 3.4 and 3.5. From these figures, it can be observed that 1Hz high pass filtering or and duration of around 0.4 sec produces robust measurements.

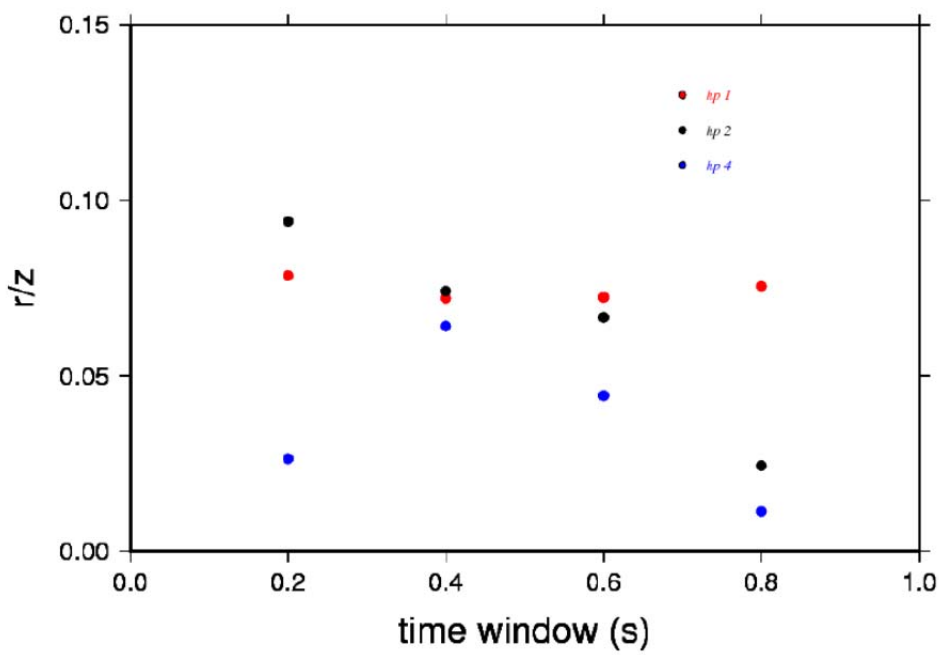


Figure 3.4. Ur/Uz measurement at station Y44A for different frequency band (red: 1Hz; black 2Hz and blue 4Hz) and time duration T (0.2-9.8 sec). Duration of 0.4 or filtering at 1Hz produces reliable automatic measurement with cross correlation

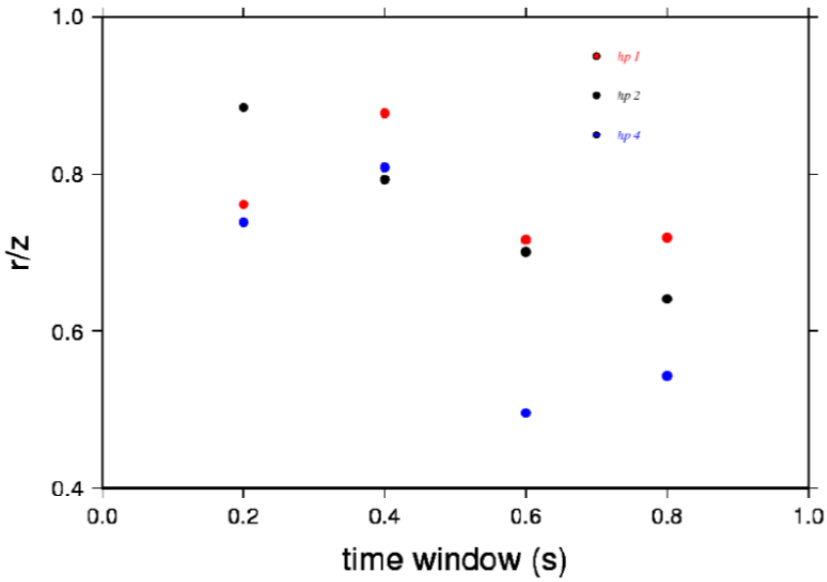


Figure 3.5. Ur/Uz measurement at station X40A for different frequency band (red: 1Hz; black 2Hz and blue 4Hz) and time duration T (0.2-9.8 sec). Duration around 0.4 or filtering at 1Hz produces reliable automatic measurement with cross correlation.

## 2. Determining subsurface shear velocity for seismic stations in CEUS

After Ur/Uz is measured, subsurface shear velocity can be estimated from equation 3 in Part I. The ray parameter *p* is computed with the CEUS crustal model and location/depth from NEIC catalog. From 2009-2012, we collected waveform data for all M3+ earthquakes in the CEUS (Figure 3.6). M2 events are not included due to low signal/ noise ratio of P waves at most stations. Waveform data from more than 1000 seismic stations and dozens of earthquakes are processed and used to infer subsurface shear velocity.

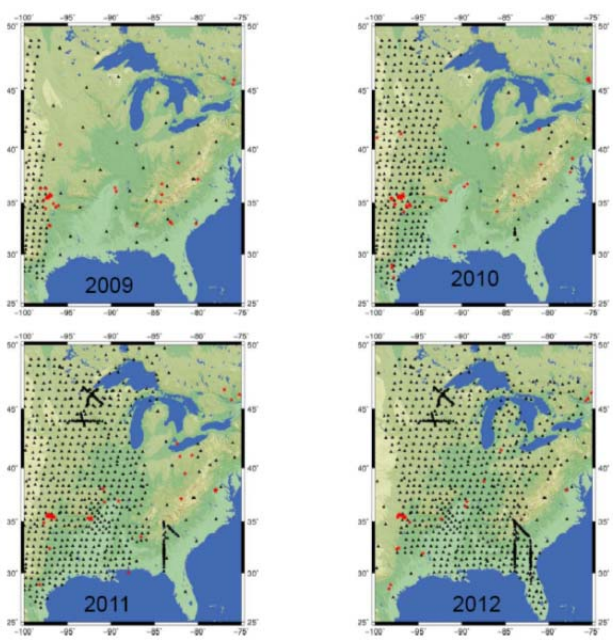


Figure 3.6. Seismic waveform data used in this study from stations (black triangle) and earthquakes (red star) for year 2009-2012.

With ray parameter p computed and Ur/Uz, we determine subsurface surface shear velocity for stations in CEUS as displayed in Figures 3.7-3.18. In Figure 3.7 – 3.12 (corresponding to different time window durations and filtering frequencies, see figure caption for details), the subsurface shear velocity is measured by taking the mean of at least three measurements (that is, P waves from at least three earthquakes are used). In Figures 3.13-3.18, the measurement is performed with P waves from at least one earthquake, so the subsurface measurement is less reliable. From these figures, it is observed that subsurface shear velocities are low for seismic stations in sedimentary basins, and are higher in mountainous regions, consistent with the geological setting.

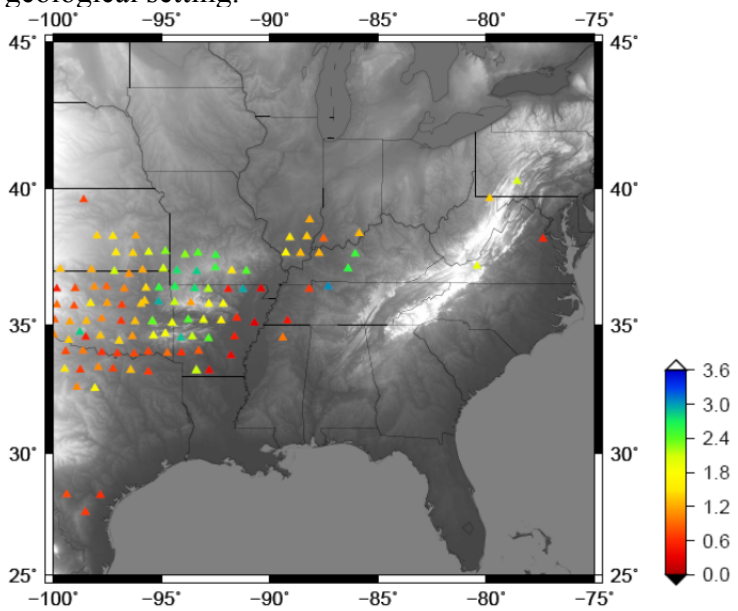


Figure 3.7. Subsurface shear velocity (Vs) measured with correlation time window of 0.3 sec and highpass frequency of 1Hz. Vs is indicated by the color bar. Vs is found to be lower than 300m/s for some stations in the Mississippi embayment. The measurement is taken as the mean of Vs determined from at least three earthquakes.

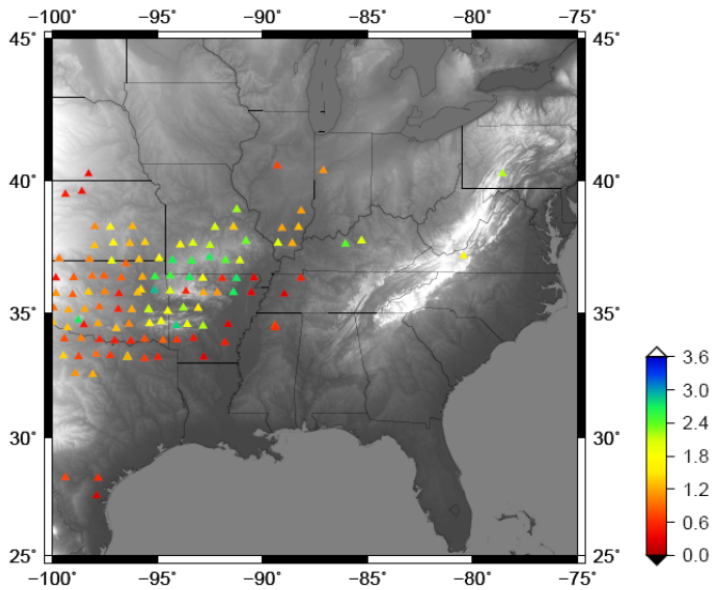


Figure 3.8. Subsurface shear velocity (Vs) measured with correlation time window of 0.3 sec and highpass frequency of 2Hz. Vs is indicated with by color bar. Vs is found to be lower than 300m/s for some stations in the Mississippi embayment. The measurement is taken as the mean of Vs determined from at least three earthquakes.

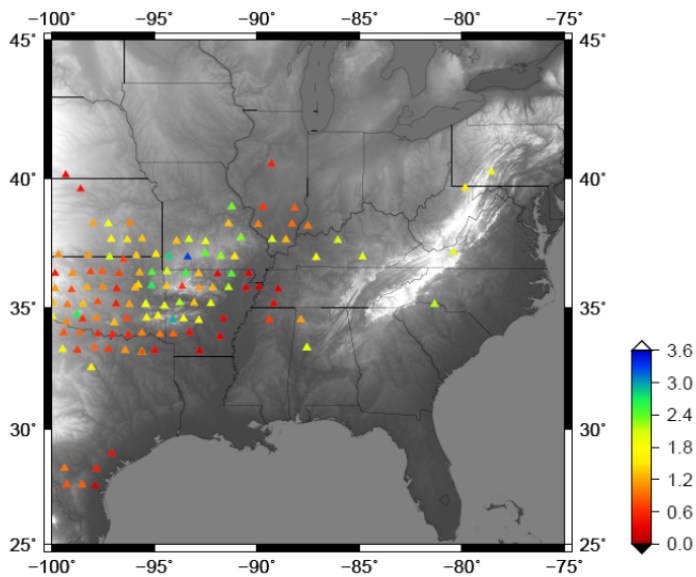


Figure 3.9. Subsurface shear velocity (Vs) measured with correlation time window of 0.3 sec and highpass frequency of 4Hz. Vs is indicated by the color bar. Vs is found to be lower than 300m/s for some stations in the Mississippi embayment. The measurement is taken as the mean of Vs determined from at least three earthquakes.

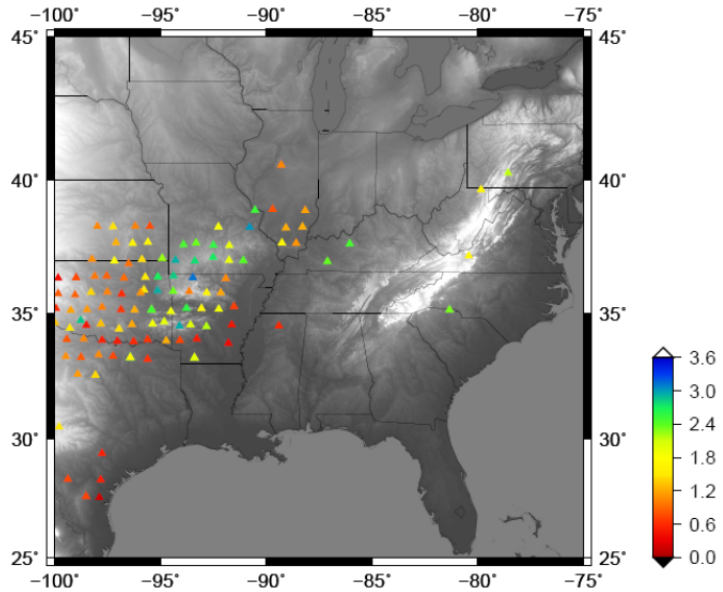


Figure 3.10. Subsurface shear velocity (Vs) measured with correlation time window of 0.5 sec and highpass frequency of 1Hz. Vs is indicated by the color bar. Vs is found to be lower than 300m/s for some stations in the Mississippi embayment. The measurement is taken as the mean of Vs determined from at least three earthquakes.

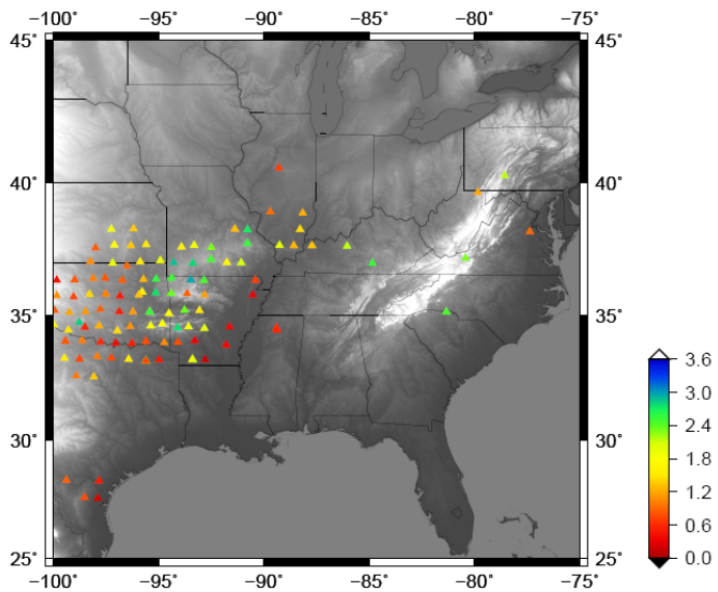


Figure 3.11. Subsurface shear velocity (Vs) measured with correlation time window of 0.5 sec and highpass frequency of 2Hz. Vs is indicated by the color bar. Vs is found to be lower than 300m/s for some stations in the Mississippi embayment. The measurement is taken as the mean of Vs determined from at least three earthquakes.

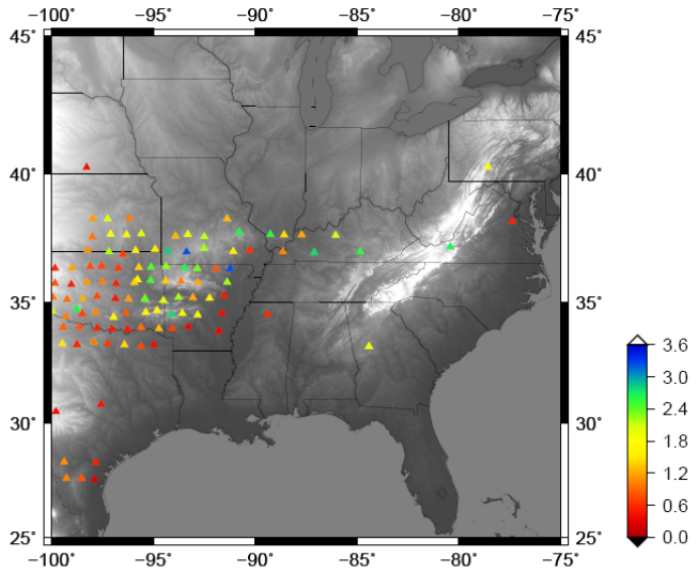


Figure 3.12. Subsurface shear velocity (Vs) measured with correlation time window of 0.5 sec and highpass frequency of 4Hz. Vs is indicated by the color bar. Vs is found to be lower than 300m/s for some stations in the Mississippi embayment. The measurement is taken as the mean of Vs determined from at least three earthquakes.

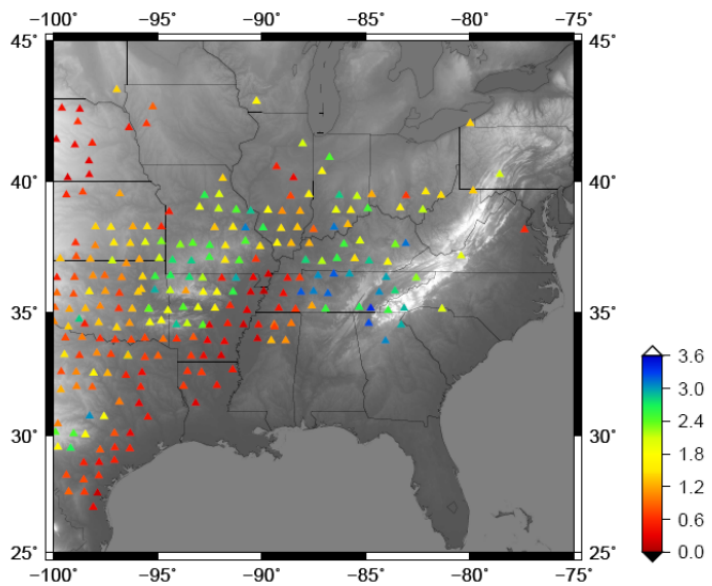


Figure 3.13. Subsurface shear velocity (Vs) measured with correlation time window of 0.3 sec and highpass frequency of 1Hz. Vs is indicated by the color bar. Vs is found to be lower than 300m/s for some stations in the Mississippi embayment. The measurement is taken as the mean of Vs determined from at least one earthquake.

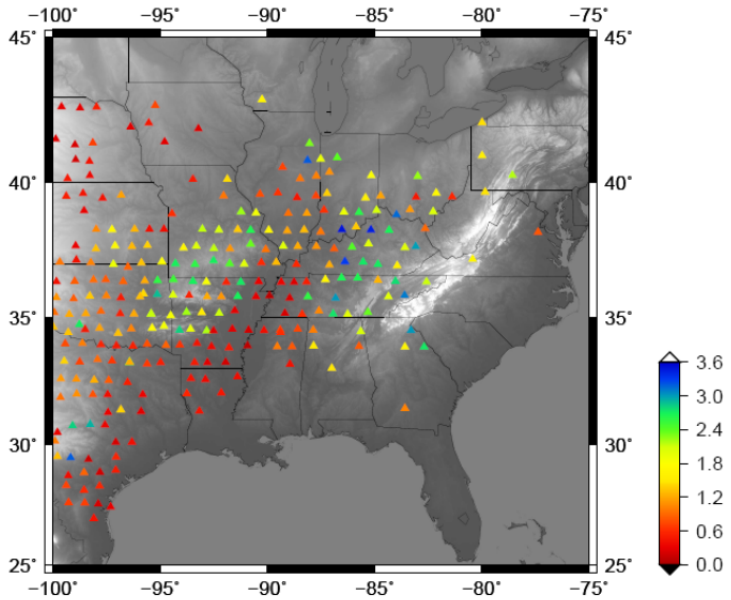


Figure 3.14. Subsurface shear velocity (Vs) measured with correlation time window of 0.3 sec and highpass frequency of 2Hz. Vs is indicated by the color bar. Vs is found to be lower than 300m/s for some stations in the Mississippi embayment. The measurement is taken as the mean of Vs determined from at least one earthquake.

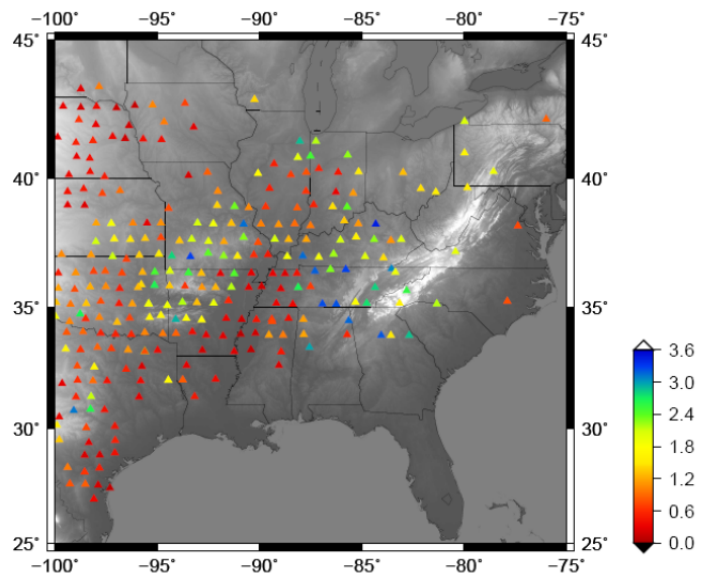


Figure 3.15. Subsurface shear velocity (Vs) measured with correlation time window of 0.3 sec and highpass frequency of 4Hz. Vs is indicated by the color bar. Vs is found to be lower than 300m/s for some stations in the Mississippi embayment. The measurement is taken as the mean of Vs determined from at least one earthquake.

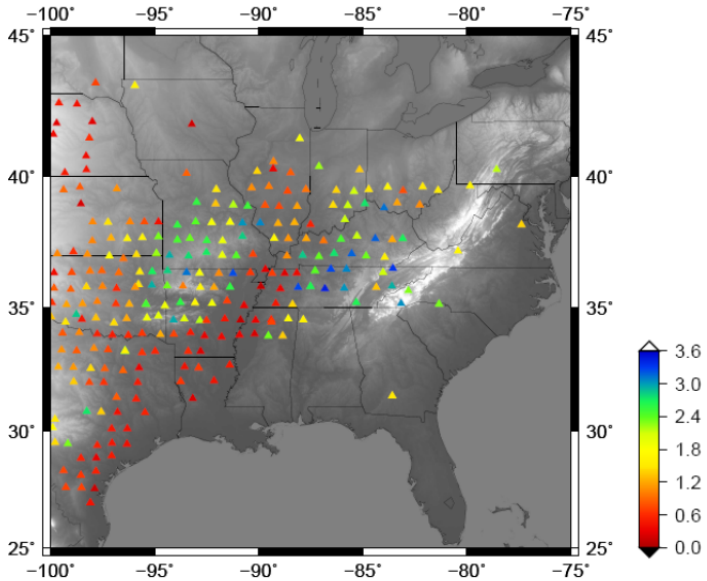


Figure 3.16. Subsurface shear velocity (Vs) measured with correlation time window of 0.5 sec and highpass frequency of 1Hz. Vs is indicated by the color bar. Vs is found to be lower than 300m/s for some stations in the Mississippi embayment. The measurement is taken as the mean of Vs determined from at least one earthquake.

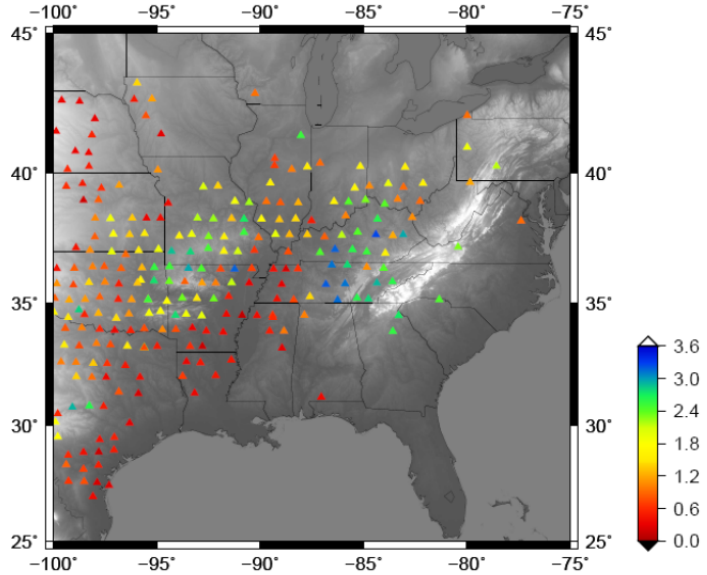


Figure 3.17. Subsurface shear velocity (Vs) measured with correlation time window of 0.5 sec and highpass frequency of 2Hz. Vs is indicated by the color bar. Vs is found to be lower than 300m/s for some stations in the Mississippi embayment. The measurement is taken as the mean of Vs determined from at least one earthquake.

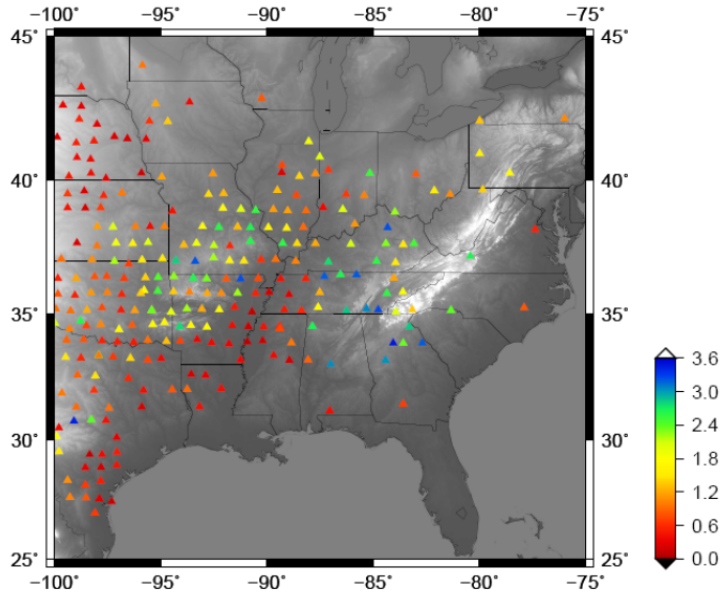


Figure 3.18. Subsurface shear velocity (Vs) measured with correlation time window of 0.5 sec and highpass frequency of 4Hz. Vs is indicated by the color bar. Vs is found to be lower than 300m/s for some stations in the Mississippi embayment. The measurement is taken as the mean of Vs determined from at least one earthquakes.

## 3. Summary

In summary, the initial portion of three component local P waves can be used to constrain subsurface shear velocity structure in a similar way to teleseismic P receiver functions, only at much higher temporal resolution and smaller spatial scale. The shear velocity just beneath the free surface can be readily estimated from the ratio $\frac{U_R}{U_Z}$ of the P wave once the ray parameter p is determined (equation 3). Of course, the depth extent of low subsurface shear velocity estimated this way depends on the source duration of vertical P. For a local earthquake with duration of 0.1 second (M3 earthquake), the shear velocity estimated from $\frac{U_R}{U_Z}$ of P is actually the average velocity $\beta$ from the free surface to depth $h = 0.1sec \times \beta$. For NEHRP site class C, that corresponds to a depth extent of 50m. The duration of vertical P can be effectively made smaller by choosing an appropriate value of the α parameter as used in most teleseismic receiver functions (Ligorria and Ammon, 1999). With additional constraints from the noise H/V ratio, the resolution of subsurface shear velocity structure can be improved.

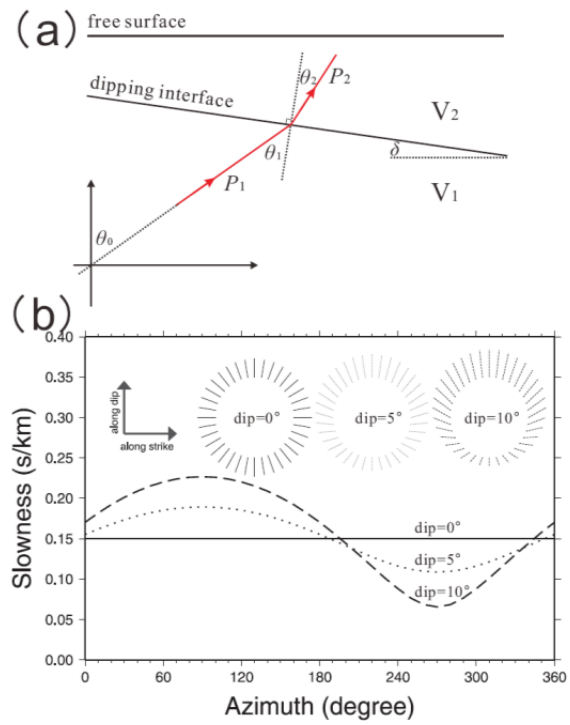


Figure 3.19. Effects of a dipping interface on the slowness of the P wave. (a) Geometry for tracing P waves. V1 and V2 are P velocities in the bedrock and sediments, and are chosen to be 2.0 km/s and 6.0 km/s respectively. (b) Changes of slowness vs back-azimuth for a flat layer (dip=0 degree, solid) and dipping layers (dip = 5 (dotted) and 10 degrees (dashed)). The three rose diagrams show effects on the slowness vector. The up-dip direction shows the largest slowness, and down-dip the smallest. Dipping interfaces also change the horizontal polarization angle of P waves.

However, we have assumed flat interfaces in estimating the velocity structures described above, and dipping layers may affect the results by changing the ray parameter. In Figure 3.19, the variation of P wave slowness with azimuth is displayed for flat and dipping interfaces. When the dip angle is 5 degrees, the change in slowness is within 30%, but when the dip angle is 10 degrees, changes of slowness can be up to 50%. Nevertheless, when earthquakes along different azimuths are used, the averaged slowness is still very close to that for flat interfaces. Therefore, it is recommended that *Uz*/*Ur* of local P wave be measured from events along different azimuths.

## DISPOSITION OF DATA SETS

We have measured subsurface shear velocity for hundred seismic stations in CEUS. In the Appendix, we list the measurement for stations for various measurement conditions (only one event used, or at least three events used, and for different frequency/time window duration combinations).

## BIBLIOGRAPHY OF ALL PUBLICATIONS RESULTING FROM THIS PROJECT

One abstract is presented at AGU 2011. Three papers have been submitted to SRL and BSSA respectively.

1. To SRL,

   Ni ,Li and Somerville, 2013

   Estimating Subsurface Shear Velocity with Radial and Vertical Ratio of Local P Waves

2. To BSSA,

   Li, Ni and Somerville, 2013

   Resolving shallow shear-wave velocity structure beneath Station CBN with waveform modeling of the Mw 5.8 Mineral, Virginia earthquake sequence

3. To BSSA,

   Kim, Hashash, Ni, Somerville, Kottke, Stewart, Silva, Rathje, and Campbell, 2013

   Shear-Wave Velocity Characterization using P-Wave Time Series in Central and Eastern North America

## ACKNOWLEDGMENTS

Seismic waveform data was provided by IRIS DMC. Discussion with Professor Youssef M. A. Hashash and his research group improved our algorithms.

## REFERENCES

Aki, K., and P. G. Richards (2002). Quantitative Seismology, Second Ed., University Science Books, Sausalito, California, ISBN 0-935702-96-2,

Al Yuncha, Z. & Luzon, F., 2000. On the horizontal-to-vertical spectral ratio in sedimentary basins, Bull. Seism. Soc. Am., 90, 1101–1106.

Ammon, C. J., The isolation of receiver effects from teleseismic P waveforms, Bull. Seism. Soc. Am., 81, 2504-2510, December 1991.

Arai, H. and K. Tokimatsu (2004). S-wave velocity profiling by inversion of microtremor H/V spectrum, Bull. Seism. Soc. Am. 94, 53—63.

Atkinson, G. M. and D. M. Boore (2006). Earthquake ground-motion prediction equations for eastern North America, Bull. Seism. Soc. Am. 96, 2181--2205.

Boore, D. M. (2003). Simulation of ground motion using the stochastic method, Pure and Applied Geophysics 160, 635—675

Boore, D. M. (2006). Determining subsurface shear-wave velocities: A review, Third International Symposium on the Effects of Surface Geology on Seismic Motion (P.-Y. Bard, E. Chaljub, C. Conrou, F. Cotton, and P. Gueguen, Editors), Grenoble, France, 30 August - 1 September 2006, Laboratoire Central des Ponts et Chauss\'ees, 67—85

Chen, K., J. Chiu, and Y. Yang (1996). Shear-wave velocity of the sedimentary basin in the upper Mississippi embayment using S-to-P converted waves, Bull. Seismol. Soc. Am. 86, 848–856.

Clitheroe, G., O. Gudmundsson, and B. L. N. Kennett (2000), The crustal thickness of Australia, J. Geophys. Res., 105(B6), 13,697–13,713, doi:10.1029/1999JB900317.

Fullerton, D.S., C.A. Bush, and J.N. Pennell (2004). Map of Surficial Deposits and Materials in the Eastern and Central United States (East of 102 west longitude). U.S. Geological Survey Geological Investigations Series I-2789.

Di Giacomo, Domenico, Maria Rosaria Gallipoli, Marco Mucciarelli, Stefano Parolai, and Sandra M. Richwalski (2005). Analysis and Modeling of HVSR in the Presence of a Velocity Inversion: The Case of Venosa, Italy. Bulletin of the Seismological Society of America 95, 2,364–2,372.

Hartzell, S., D. Carver, R. A. Williams, R. Harmsen, and A. Zerva (2001). Site response, shallow shear-wave velocity, and damage in Los Gatos, California, from the 1989 Loma Prieta earthquake. Bulletin of the Seismological Society of America 93, 443–464.

Julia, J., Ammon, C.J., Herrmann, R.B. & Correig, A.M., 2000. Joint inversion of receiver function and surface wave dispersion observations, Geophys. J. Int., 143, 1–19.

Kim, B., Y. Hashash, S. Ni, P. Somerville, A. Kottke, J. Stewart, W. Silva, E. Rathje, and K. Campell (2013). Shear-wave velocity characterization using p-wave time series in Central and Eastern North America. Unpublished manuscript.

Lachet, C. & Bard, P.-Y., 1994. Numerical and theoretical investigations on the possibilities and limitations of Nakamura's technique, J. Phys. Earth, 42, 377–397.

Langston, C A., S Chiu, L. Zack, P. Bodin, S Horton, 2009, Array Observations of Microseismic Noise and the Nature of H/V in the Mississippi Embayment, Bulletin Of The Seismological Society Of America 99: 2893-291

Langston, C. A. (1989). Scattering of teleseismic body waves under Pasadena, California, J. Geophys. Res. 94, 1935–1951.

Langston, C. A. (2003). Local earthquake wave propagation through Mississippi embayment sediments: I. Body wave phases and local site responses, Bull. Seismol. Soc. Am. 93, 2664–2684.

Lermo, J., and F. J. Chávez-García (1993). Site effect evaluation using spectral ratios with only one station, Bull. Seismol. Soc. Am. 83, 1574–1594.

Ligorria, J. P., and C. J. Ammon (1999), Iterative deconvolution and receiver-function estimation, Bull. Seismol. Soc. Am., 89, 1395– 1400.

Li, Z. W., Hao, T. Y., Xu, Y., Xu, Y., Roecker, S. (2010). A global optimizing approach for waveform inversion of receiver functions. Computers & Geosciences, 36, 871-880.

Louie, J.N. (2001). Faster, better: Shear-wave velocity to 100 meters depth from refraction microtremor arrays, Bull. Seism. Soc. Am. 91, 347—364.

Ni, S. and P. Somerville (2013). Estimating shallow shear wave profiles for site response estimation using local P wave seismograms, and application in the Central United States. Draft manuscript.

Nakamura, Y. (1989). A method for dynamic characteristic estimation of subsurface using microtremor on the ground surface, Q. Rep. Railway Tech. Res. Inst. 30, 25–33.

Nakamura, Y., 2000. Clear identification of fundamental idea of Nakamura's technique and its applications, Proceedings of the 12th World Conference on Earthquake Engineering, Auckland, New Zealand.

Odum, J. K., Stephenson, W. J., and Williams, R. A., 2010, Predicted and Observed Spectral Response from Collocated Shallow, Active and Passive-Source Vs Data at Five ANSS Sites, Illinois and Indiana, USA, in preparation for SRL.

Picozzi, M., Parolai, S., & Richwalski, S.M., 2005. Joint inversion of H/V ratios and dispersion curves from seismic noise: Estimating the S-wave velocity of bedrock. Geoph. Res. Lett., 32, No.11 doi: 10.1029/2005GL022878

Read K, E Naggar, D Eaton,2008,Site-Response Spectra for POLARIS Station Sites in Southern Ontario and Quebec ,Seismological Research Letters 2008 79: 776-784

Sambridge, M. S. (1999a). Geophysical inversion with a neighbourhood algorithm. I. Searching a parameter space, Geophys. J. Int. 138, 479–494.

Sambridge, M. S. (1999b). Geophysical inversion with a neighbourhood algorithm. II. Appraising the ensemble, Geophys. J. Int. 138, 727– 746.

Lozano, L., S. M. Herraiz, and K. Singh (2008). Site effect study in central

Mexico using H/V and SSR techniques: Independence of seismic site effects on source characteristics, Soil Dyn. Earthq. Eng. 29, 504–516,doi 10.1016/J.soildyn.2008.05.009.

Stephenson, W. J., J. N. Louie, S. Pullammanappallil, R. A. Williams, and J. K. Odum (2005). Blind shear-wave velocity comparison of ReMi and MASW results with boreholes to 200 m in Santa Clara Valley: Implications for earthquake ground-motion assessment, Bull. Seism. Soc. Am. 95, 2506–-2516.

Wald, L. A, and J. Mori (2000). Evaluation of methods for estimating linear site-response amplifications in the Los Angeles region. Bulletin of the Seismological Society of America 90, S32S42.

Withers, M.M. (2007). Mid-America ShakeMap: a Large Regional Implementation. Final Technical Report, USGS Award No. 06HQGR0048.

Appendix

Table of measured subsurface shear velocity with initial P waves

Remarks

(1) Velocity in m/s

(2) 0.3s+1Hz refers to correlation window of 0.3 sec and high pass filtering with 1 Hz. So are the other combinations of time window and filter band.

Table 1. Measured Subsurface Vs with P wave from at least three earthquakes (in m/s)

| STATION | NETWORK | Vs(0.3s+1hz) | Vs(0.3s+2hz) | Vs(0.3s+4hz) | Vs(0.5s+1hz) | Vs(0.5s+2hz) | Vs(0.5s+4hz) |
|---|---|---|---|---|---|---|---|
| 034A | TA | | | 802 | | | 1076 |
| 133A | TA | 1038 | 1089 | | 1126 | 989 | |
| 134A | TA | 1700 | 1225 | 1687 | 1427 | 1350 | |
| 435B | TA | | | | | | 432 |
| 635A | TA | | | | 536 | | |
| 736A | TA | | | 401 | | | |
| 833A | TA | 751 | 724 | 977 | 732 | 865 | 1077 |
| 835A | TA | 610 | 573 | 504 | 529 | 506 | 507 |
| 933A | TA | | | 786 | | | 1005 |
| 934A | TA | 665 | | 842 | 715 | 770 | 801 |
| BLA | US | 1960 | 1687 | 1965 | 1704 | 2313 | 2676 |
| CBN | US | 553 | | | | 906 | 534 |
| HDIL | US | | 718 | 517 | 1036 | 701 | |
| JCT | US | | | | 1495 | | 386 |
| KMSC | TA | | | 2177 | 2320 | 2461 | |
| KVTX | US | | 209 | 212 | 168 | 221 | 234 |
| LONY | US | 2748 | 2763 | 2869 | 2773 | 2789 | 2771 |
| MCWV | US | 1366 | | 1548 | 1671 | 1201 | |
| MIAR | US | 2133 | 1945 | 1780 | 2009 | 1893 | 1698 |
| O31A | TA | | | 357 | | | |
| O32A | TA | | 352 | | | | 387 |
| O56A | TA | 2062 | 2178 | 1904 | 2154 | 2157 | 1767 |
| OXF | US | 963 | 732 | 662 | 586 | 658 | 581 |
| P31A | TA | | 514 | | | | |
| P32A | TA | 706 | 436 | 451 | | | |
| Q41A | TA | | 2235 | 2344 | | | |
| Q42A | TA | | | | 2528 | | |
| Q43A | TA | | | 643 | 784 | 922 | |
| Q45A | TA | 1203 | 1148 | 830 | 1159 | 1230 | |

| | | | | | | | |
|---|---|---|---|---|---|---|---|
| R33A | TA | 1388 | 1041 | 1168 | 1038 | | 1150 |
| R34A | TA | 1488 | 1702 | 1867 | 1472 | 1896 | 2032 |
| R35A | TA | 1193 | 1254 | 1015 | 1023 | 1344 | 1000 |
| R36A | TA | | | | 763 | | |
| R40A | TA | | 2082 | | 1860 | | |
| R41A | TA | | 1358 | 1303 | | 1310 | 1285 |
| R42A | TA | | | | 3029 | 2722 | |
| R43A | TA | | | 1009 | | | |
| R44A | TA | 1492 | 1183 | | 1216 | | |
| R45A | TA | 1342 | 1286 | 906 | 1235 | 1430 | |
| R46A | TA | 853 | | 968 | | | |
| R48A | TA | 1281 | | | | | |
| S33A | TA | | 1305 | | | 844 | 957 |
| S34A | TA | 1525 | 1746 | 1676 | 1235 | 1810 | 1872 |
| S35A | TA | 1400 | 1272 | 1479 | 1658 | 1352 | 1647 |
| S36A | TA | 1981 | 1383 | 1348 | 1646 | 1539 | 2017 |
| S37A | TA | 2304 | | | | | |
| S38A | TA | 2283 | 1683 | 1320 | 2481 | 1641 | 1284 |
| S39A | TA | 2426 | 2035 | 2108 | 2358 | 1909 | 1904 |
| S40A | TA | 2559 | 2147 | 1993 | 2575 | 2314 | 2144 |
| S41A | TA | | | | 1938 | | |
| S42A | TA | | 2363 | 2292 | | 2548 | 2633 |
| S44A | TA | 1688 | 2017 | 2087 | 1704 | 1977 | 2600 |
| S45A | TA | 1280 | 1216 | 1264 | 1099 | 1262 | 1440 |
| S46A | TA | 1251 | | | | 1351 | 1198 |
| S48A | TA | 2535 | 2426 | 2098 | 2479 | 2152 | 2093 |
| S49A | TA | | 2014 | | | | |
| SFIN | TA | | 1095 | | | | |
| T31A | TA | 1305 | 959 | 1052 | | | |
| T33A | TA | 1210 | 1019 | 1122 | 1076 | 1066 | 1079 |
| T34A | TA | 2114 | 1933 | 2116 | 1792 | 1960 | 2203 |
| T35A | TA | 1098 | 872 | 691 | 938 | 892 | 691 |
| T36A | TA | 1200 | 1327 | 1368 | 1448 | 1559 | 1542 |
| T37A | TA | 2087 | 1803 | 1562 | 2246 | 1911 | 1501 |
| T38A | TA | 2760 | 2710 | 2809 | 2945 | 2885 | 2828 |
| T39A | TA | 2843 | 2603 | 3285 | 2782 | 2806 | 3223 |
| T40A | TA | 2556 | 2716 | 2395 | 2728 | 2494 | 2216 |
| T41A | TA | 1504 | 2440 | 2265 | 1941 | 1681 | |
| T42A | TA | 2436 | 2010 | 1535 | 2426 | 2082 | 1502 |
| T43A | TA | | | | | | 613 |
| T45A | TA | | | | | | 1022 |

| | | | | | | | |
|---|---|---|---|---|---|---|---|
| T47A | TA | | | 1850 | 2373 | | 2770 |
| T48A | TA | 2590 | | | | | |
| T50A | TA | | | 2018 | | 2548 | 2604 |
| TUL1 | TA | 1345 | 1423 | 1421 | 1485 | 1626 | 1715 |
| U30A | TA | | | 403 | | | |
| U31A | TA | 508 | 416 | 490 | 388 | 430 | 542 |
| U32A | TA | 760 | 838 | 1085 | 745 | 838 | 1179 |
| U33A | TA | 1077 | 922 | 705 | 968 | 1009 | 786 |
| U34A | TA | 876 | 833 | 813 | 863 | 810 | 756 |
| U35A | TA | 1031 | 864 | 710 | 908 | 846 | 680 |
| U36A | TA | 1424 | 1208 | 1243 | 1517 | 1264 | 1384 |
| U37A | TA | 2571 | 2594 | 2485 | 2709 | 2571 | 2435 |
| U38A | TA | 2675 | 2529 | 2040 | 2833 | 2524 | 2268 |
| U39A | TA | 2780 | 2709 | 2541 | 3130 | 2970 | 2652 |
| U40A | TA | 2185 | 1853 | 1300 | | 2469 | 2332 |
| U41A | TA | 456 | 539 | 279 | 1057 | | 808 |
| U42A | TA | 2958 | 2735 | 2443 | | | 3239 |
| U43A | TA | 319 | 316 | 276 | | 703 | |
| U46A | TA | 675 | 517 | | | | |
| U47A | TA | 3048 | | | | | |
| V30A | TA | | 432 | 549 | | | 488 |
| V31A | TA | 900 | 1103 | 1151 | 842 | 1087 | 799 |
| V32A | TA | 762 | 842 | 756 | 868 | 724 | 528 |
| V33A | TA | 1548 | 1350 | 1224 | 1411 | 1423 | 1120 |
| V34A | TA | 1142 | 1014 | 1056 | 1028 | 1021 | 1007 |
| V35A | TA | 678 | 490 | 502 | 582 | 510 | 537 |
| V36A | TA | 1356 | 1304 | 1274 | 1109 | 1330 | 1379 |
| V37A | TA | 2937 | 2890 | 2671 | 2941 | 2766 | 2521 |
| V38A | TA | 2128 | 2030 | 1343 | 2349 | 2355 | 1366 |
| V39A | TA | 1150 | 539 | 635 | 991 | 852 | 1013 |
| V40A | TA | 1791 | 1207 | 1108 | 1689 | 1154 | 1201 |
| V41A | TA | 1765 | 1114 | 1261 | 1196 | | |
| V42A | TA | | 2707 | 2172 | | | 2234 |
| V43A | TA | | 290 | 256 | | 303 | |
| V44A | TA | | | 177 | | | |
| V45A | TA | | 225 | 256 | | | |
| W31A | TA | 863 | 927 | 1310 | 628 | 852 | 929 |
| W32A | TA | 1166 | 1203 | 951 | 1170 | 1189 | 922 |
| W33A | TA | 1281 | 1189 | 1321 | 1130 | 1126 | 1220 |
| W34A | TA | 1037 | 883 | 765 | 1005 | 864 | 748 |
| W35A | TA | 641 | 529 | 480 | 657 | 515 | 482 |

| | | | | | | | |
|---|---|---|---|---|---|---|---|
| W36A | TA | 1294 | 1199 | 1147 | 1227 | 1133 | 1152 |
| W37A | TA | 2093 | 2049 | 1799 | 2161 | 2118 | 1637 |
| W37B | TA | 2408 | 2135 | 1894 | 2512 | 2553 | 2383 |
| W38A | TA | 1906 | 1866 | 1926 | 1899 | 1809 | 1989 |
| W39A | TA | 2443 | 2228 | 2185 | 2600 | 2351 | 2218 |
| W40A | TA | 1929 | 1533 | 1300 | 1700 | 1501 | 1219 |
| W41B | TA | 1645 | | 1940 | 1888 | | 1693 |
| W42A | TA | 563 | | | 693 | | 474 |
| W43A | TA | 253 | | | | | |
| W45A | TA | 435 | | 325 | | | |
| WMOK | US | 2843 | 2726 | 2689 | 2860 | 2828 | 2646 |
| X30A | TA | 1453 | | 871 | | 625 | 1040 |
| X31A | TA | 1041 | 1335 | 1859 | 1333 | 1715 | 2021 |
| X32A | TA | 1358 | 1326 | 1024 | 1490 | 1488 | 1001 |
| X33A | TA | 502 | 477 | 595 | 460 | 540 | 711 |
| X34A | TA | 1330 | 1176 | 1022 | 1310 | 1242 | 1035 |
| X35A | TA | 1406 | 1313 | 1288 | 1450 | 1437 | 1683 |
| X36A | TA | 1124 | 1032 | 728 | 1198 | 1096 | 829 |
| X37A | TA | 1852 | 1762 | 1668 | 1890 | 1861 | 1716 |
| X38A | TA | 1822 | 1875 | 1723 | 1987 | 1827 | 1667 |
| X39A | TA | 2879 | 2826 | 2936 | 2960 | 2778 | 2784 |
| X40A | TA | 2416 | 2189 | 1760 | 2174 | 1972 | 1758 |
| X42A | TA | 493 | 269 | 314 | 443 | 367 | 390 |
| X45A | TA | | 603 | | | 569 | |
| X47A | TA | | | 1155 | | | |
| Y31A | TA | | 917 | | | | |
| Y32A | TA | 744 | 755 | 807 | 808 | 808 | 868 |
| Y33A | TA | 980 | 1000 | 886 | 1046 | 1005 | 796 |
| Y34A | TA | 617 | 560 | 531 | 532 | 582 | 530 |
| Y35A | TA | 658 | 484 | 529 | 489 | 353 | 506 |
| Y36A | TA | 724 | 530 | 560 | 579 | 510 | 472 |
| Y37A | TA | 710 | 777 | 1024 | 647 | 762 | 919 |
| Y38A | TA | 916 | 869 | 965 | 1223 | 1051 | 1301 |
| Y39A | TA | 610 | 644 | 861 | 717 | 759 | 708 |
| Y40A | TA | 809 | 446 | 379 | 479 | 316 | 332 |
| Y42A | TA | 334 | 484 | 263 | 354 | 350 | 321 |
| Z31A | TA | 1431 | | | | | |
| Z32A | TA | 1494 | 1399 | 1683 | 1088 | 1586 | 1498 |
| Z33A | TA | 668 | 712 | 639 | 828 | 735 | 563 |
| Z34A | TA | 1048 | 913 | 870 | 1060 | 990 | 962 |
| Z35A | TA | 688 | 656 | 669 | 736 | 759 | 659 |

| | | | | | | | |
|---|---|---|---|---|---|---|---|
| Z36A | TA | 1290 | 1211 | 1104 | 1639 | 1528 | 1421 |
| Z37A | TA | 675 | 673 | 758 | 627 | 715 | 726 |
| Z38A | TA | | 512 | 355 | | 478 | 354 |
| Z41A | TA | 362 | 268 | 188 | | 152 | |

Table 2. Measured Subsurface Vs with P wave from one or more earthquakes (in m/s)

| STATION | NETWORK | Vs(0.3s+1hz) | Vs(0.3s+2hz) | Vs(0.3s+4hz) | Vs(0.5s+1hz) | Vs(0.5s+2hz) | Vs(0.5s+4hz) |
|---|---|---|---|---|---|---|---|
| 034A | TA | 468 | 612 | 802 | 415 | 473 | 1076 |
| 035A | TA | 341 | 427 | 345 | 423 | 367 | 668 |
| 133A | TA | 1038 | 1089 | 764 | 1126 | 989 | 863 |
| 134A | TA | 1700 | 1225 | 1687 | 1427 | 1350 | 1480 |
| 135A | TA | 1231 | 833 | | 836 | 631 | |
| 136A | TA | 506 | 514 | 543 | 857 | 460 | 577 |
| 137A | TA | 360 | | 214 | 318 | | |
| 140A | TA | 632 | 446 | 284 | 424 | 333 | 212 |
| 141A | TA | 662 | 363 | | 674 | 458 | 288 |
| 143A | TA | 461 | 392 | | 484 | 460 | |
| 146A | TA | | | 238 | | | |
| 231A | TA | 720 | 722 | 842 | 690 | 761 | 612 |
| 232A | TA | 1222 | 941 | 276 | | | 974 |
| 233A | TA | 1012 | 1081 | 623 | 1363 | 1383 | |
| 234A | TA | 838 | 789 | 913 | 736 | 918 | 640 |
| 237A | TA | 524 | 326 | 356 | 492 | 395 | 404 |
| 239A | TA | | | 1736 | | | 807 |
| 240A | TA | 654 | 567 | 823 | 646 | 674 | 893 |
| 242A | TA | 457 | 451 | 365 | 434 | 454 | 400 |
| 333A | TA | | | 556 | | | 902 |
| 334A | TA | | | 2132 | | | |
| 335A | TA | | 316 | | | | 932 |
| 336A | TA | 975 | 1396 | | 838 | 785 | |
| 337A | TA | 295 | 264 | 276 | 507 | 221 | 216 |
| 341A | TA | 253 | 445 | 471 | 225 | 343 | 416 |
| 433A | TA | | 2825 | 3118 | | 2927 | 3425 |
| 434A | TA | 3048 | 2932 | 2638 | 2747 | 2632 | 2400 |
| 435B | TA | 1805 | 332 | 424 | 1371 | 491 | 432 |
| 436A | TA | | | | 411 | | |
| 438A | TA | 442 | | | 537 | | |
| 531A | TA | | | | 844 | 862 | |
| 532A | TA | 2428 | 993 | 1606 | 1760 | 1837 | 1823 |
| 533A | TA | 2480 | | | | | |

| | | | | | | | |
|---|---|---|---|---|---|---|---|
| 534A | TA | 1785 | | 738 | | | |
| 536A | TA | 780 | 212 | 432 | 471 | | 276 |
| 537A | TA | 319 | 392 | | 417 | 287 | |
| 631A | TA | 1373 | | | 2291 | | |
| 632A | TA | 1699 | 1301 | 1344 | 1434 | 1798 | 1542 |
| 633A | TA | 2675 | 3198 | | 2316 | | |
| 634A | TA | | 156 | 255 | | | 112 |
| 635A | TA | 807 | | | 536 | 416 | 375 |
| 636A | TA | 537 | 562 | 520 | 452 | 528 | 495 |
| 637A | TA | 540 | | | 405 | | |
| 733A | TA | | 386 | | | 584 | |
| 734A | TA | 516 | 870 | 222 | 537 | 399 | 280 |
| 735A | TA | 374 | 194 | 209 | 292 | 154 | 187 |
| 736A | TA | 508 | 493 | 401 | 482 | 482 | 436 |
| 833A | TA | 751 | 724 | 977 | 732 | 865 | 1077 |
| 834A | TA | 742 | 588 | 640 | 654 | 692 | 672 |
| 835A | TA | 610 | 573 | 504 | 529 | 506 | 507 |
| 933A | TA | 852 | 688 | 786 | 705 | 645 | 1005 |
| 934A | TA | 665 | 695 | 842 | 715 | 770 | 801 |
| 936A | TA | 760 | 283 | 107 | | 253 | 156 |
| ABTX | TA | | 1128 | | 1233 | 999 | |
| ACSO | US | | 2250 | 1300 | | 1608 | 825 |
| AMTX | US | 606 | 500 | 348 | 577 | | |
| BGNE | TA | 515 | 692 | 568 | 629 | 547 | 492 |
| BINY | US | | | 862 | | | 1049 |
| BLA | US | 1960 | 1687 | 965 | 704 | 313 | 676 |
| BRAL | US | | | | | 361 | 385 |
| CBN | US | 553 | 807 | 733 | 395 | 906 | 534 |
| CNNC | US | | | 768 | | | 812 |
| ERPA | US | 1395 | 1454 | 2055 | | 918 | 1325 |
| HDIL | US | 523 | 718 | 517 | 1036 | 701 | 732 |
| I34A | TA | | | | | | 960 |
| J27A | TA | | | 220 | | | 375 |
| J28A | TA | | | 700 | | | 794 |
| J29A | TA | | 1335 | | | 1375 | |
| J31A | TA | | | 263 | | | 428 |
| J32A | TA | | | 986 | 706 | | |
| J33A | TA | 1402 | | | | | |
| J34A | TA | | | | 1645 | 1408 | |
| JCT | US | 1002 | 314 | 348 | 495 | 577 | 386 |
| JFWS | US | 1686 | 1659 | 1400 | | 930 | 813 |

| | | | | | | | |
|---|---|---|---|---|---|---|---|
| K28A | TA | 1140 | 1125 | 884 | 934 | 1028 | 757 |
| K29A | TA | 234 | 223 | 228 | | | |
| K30A | TA | 411 | 290 | 315 | 494 | 322 | 321 |
| K31A | TA | 310 | 274 | 199 | 421 | 309 | 288 |
| K32A | TA | | 521 | 378 | | | |
| K33A | TA | | | 150 | | | |
| K34A | TA | | | 141 | | 471 | |
| K35A | TA | 861 | 738 | 1035 | | 1154 | 1193 |
| K37A | TA | | | 711 | | | 359 |
| KMSC | TA | 2011 | | 2177 | 2320 | 2461 | 2389 |
| KVTX | US | 133 | 209 | 212 | 168 | 221 | 234 |
| L29A | TA | 431 | 287 | 264 | 268 | 253 | 213 |
| L30A | TA | | | | 263 | | |
| L31A | TA | 633 | | 647 | | | 566 |
| L32A | TA | | | 299 | 266 | 301 | 281 |
| L34A | TA | 461 | 263 | 196 | | | |
| L35A | TA | 665 | 471 | | | 786 | 639 |
| L36A | TA | | | 991 | | | 1365 |
| LBNH | US | | 2778 | 2766 | | 2390 | |
| LONY | US | 2748 | 2763 | 2869 | 2773 | 2789 | 2771 |
| LRAL | US | | 1489 | | | | 3047 |
| M28A | TA | 457 | 425 | 396 | 334 | 339 | 312 |
| M29A | TA | 267 | 229 | 243 | 303 | 281 | 267 |
| M30A | TA | 266 | 248 | 295 | 371 | 356 | 221 |
| M31A | TA | 372 | 221 | 518 | | | 522 |
| M33A | TA | | | 353 | | | 235 |
| M34A | TA | | | 171 | | | 200 |
| M35A | TA | | | 398 | | | 269 |
| M36A | TA | | 273 | 401 | | 269 | |
| M44A | TA | 2098 | 2314 | 2891 | 1843 | 2547 | 1871 |
| M45A | TA | | | 2173 | | | |
| MCWV | US | 1366 | 1475 | 1548 | 1671 | 1201 | 1383 |
| MIAR | US | 2133 | 1945 | 1780 | 2009 | 1893 | 1698 |
| N27A | TA | | | 425 | | | 526 |
| N28A | TA | | | 199 | | | 306 |
| N29A | TA | | 652 | 664 | | | 488 |
| N31A | TA | | 195 | 289 | | 317 | 374 |
| N32A | TA | 261 | 428 | 410 | 378 | 346 | 373 |
| N44A | TA | | 3205 | 1991 | | | |
| N45A | TA | | 1951 | 2503 | | | 2043 |
| N46A | TA | 2460 | 2405 | | | | |

| | | | | | | | |
|---|---|---|---|---|---|---|---|
| N47A | TA | | | 2267 | | | |
| N54A | TA | | 1589 | 1650 | | 1920 | 1629 |
| O28A | TA | | | 221 | | | 207 |
| O30A | TA | 286 | 275 | 395 | | | |
| O31A | TA | 227 | 469 | 357 | 487 | 592 | 486 |
| O32A | TA | 321 | 352 | 399 | 450 | 512 | 387 |
| O33A | TA | | | 484 | | | 266 |
| O35A | TA | | | | | | 183 |
| O36A | TA | | | | | 1094 | 1171 |
| O38A | TA | | 481 | 223 | 856 | | |
| O39A | TA | | | 850 | | | 1118 |
| O40A | TA | 1398 | 1440 | | | | |
| O42A | TA | | | 1749 | 1403 | | |
| O43A | TA | | | | 311 | 677 | 246 |
| O44A | TA | 340 | 957 | 681 | 833 | 988 | 1395 |
| O45A | TA | | 1006 | 792 | | 1556 | 1089 |
| O47A | TA | | | 454 | | | |
| O48A | TA | | 1829 | 1546 | 1363 | 1667 | 2530 |
| O56A | TA | 2062 | 2178 | 1904 | 2154 | 2157 | 1767 |
| OGNE | US | | 729 | 685 | | 593 | 452 |
| OXF | US | 963 | 732 | 662 | 586 | 658 | 581 |
| P27A | TA | | | 993 | | | 523 |
| P29A | TA | | | 305 | | | |
| P30A | TA | 526 | 619 | 359 | 446 | | |
| P31A | TA | 550 | 514 | 437 | 898 | 618 | 672 |
| P32A | TA | 706 | 436 | 451 | 843 | 478 | 236 |
| P33A | TA | | 426 | 715 | | 629 | 569 |
| P34A | TA | 1176 | 1168 | 929 | 1089 | 1146 | 973 |
| P39B | TA | 2636 | | | | 2038 | 1435 |
| P40A | TA | 2015 | 957 | 1048 | 1501 | 1390 | 1263 |
| P42A | TA | | 768 | | 1068 | | |
| P43A | TA | | 635 | 509 | 984 | 1596 | 1294 |
| P44A | TA | 719 | 455 | | 745 | | 736 |
| P45A | TA | 1666 | 719 | 645 | 951 | | |
| P46A | TA | | 1371 | | | | |
| P47A | TA | 2840 | | 312 | 1396 | | 666 |
| P48A | TA | 2133 | 1621 | 1131 | 2107 | 1689 | 1013 |
| P49A | TA | 1217 | 1181 | | 1485 | 1064 | |
| P50A | TA | | | | 1700 | 1930 | |
| P51A | TA | 666 | 474 | | 772 | 910 | |
| P52A | TA | 1511 | 1730 | 1448 | 1500 | 1640 | 1556 |

| | | | | | | | |
|---|---|---|---|---|---|---|---|
| P53A | TA | 1441 | 568 | 1572 | 1557 | | 1060 |
| PAL | D | 3170 | | 433 | 112 | | |
| Q28A | TA | | | 176 | | | 255 |
| Q30A | TA | | | 750 | | | |
| Q31A | TA | | | 282 | | | 452 |
| Q32A | TA | | 311 | 244 | 209 | 183 | 211 |
| Q33A | TA | | | | | 842 | 691 |
| Q37A | TA | 477 | 612 | 758 | | 370 | 427 |
| Q39A | TA | 1925 | | | 2578 | | |
| Q40A | TA | 2133 | | 1386 | 1326 | | 1725 |
| Q41A | TA | 2453 | 2235 | 2344 | 2176 | 1866 | 2023 |
| Q42A | TA | 2875 | 1885 | 1052 | 2528 | 2222 | 2566 |
| Q43A | TA | 1794 | | 643 | 784 | 922 | 1138 |
| Q44A | TA | 1080 | 921 | | 737 | 821 | 1156 |
| Q45A | TA | 1203 | 1148 | 830 | 1159 | 1230 | 901 |
| Q46A | TA | | 628 | 518 | | | 357 |
| Q47A | TA | 1931 | 1939 | 1457 | 1441 | 1618 | 2039 |
| Q48A | TA | 1600 | 2626 | 2397 | 2123 | 2434 | |
| Q49A | TA | 2502 | 2100 | | 2755 | 2320 | |
| Q50A | TA | | 3159 | | 3135 | 2419 | 2240 |
| Q51A | TA | 1618 | 1132 | | 1172 | 1013 | |
| Q52A | TA | 2152 | 2057 | | 1066 | 904 | |
| R33A | TA | 1388 | 1041 | 1168 | 1038 | 1034 | 1150 |
| R34A | TA | 1488 | 1702 | 1867 | 1472 | 1896 | 2032 |
| R35A | TA | 1193 | 1254 | 1015 | 1023 | 1344 | 1000 |
| R36A | TA | 1473 | 403 | 285 | 763 | 320 | 384 |
| R37A | TA | 554 | 388 | 1088 | 414 | 391 | 1013 |
| R38A | TA | | | | 2577 | | |
| R39A | TA | | 2150 | 2091 | 2427 | 2179 | 1743 |
| R40A | TA | 1321 | 2082 | 1886 | 1860 | 2245 | 2619 |
| R41A | TA | 1541 | 1358 | 1303 | 1844 | 1310 | 1285 |
| R42A | TA | 3095 | 2657 | 3145 | 3029 | 2722 | 2660 |
| R43A | TA | 2623 | 1702 | 1009 | 3076 | 1741 | 1665 |
| R44A | TA | 1492 | 1183 | 1104 | 1216 | 1325 | 1640 |
| R45A | TA | 1342 | 1286 | 906 | 1235 | 1430 | 893 |
| R46A | TA | 853 | 963 | 968 | 535 | 489 | |
| R47A | TA | 3124 | 3494 | | | | |
| R48A | TA | 1281 | 1348 | 1343 | 2119 | 1018 | 1116 |
| R49A | TA | | 3441 | 1117 | | | |
| R50A | TA | | 2701 | 3438 | | 2638 | 3228 |
| R52A | TA | | 901 | | | 1077 | |

| | | | | | | | |
|---|---|---|---|---|---|---|---|
| S32A | TA | 615 | 307 | | | | 230 |
| S33A | TA | 1026 | 1305 | 2107 | 1026 | 844 | 957 |
| S34A | TA | 1525 | 1746 | 1676 | 1235 | 1810 | 1872 |
| S35A | TA | 1400 | 1272 | 1479 | 1658 | 1352 | 1647 |
| S36A | TA | 1981 | 1383 | 1348 | 1646 | 1539 | 2017 |
| S37A | TA | 2304 | | 731 | 2326 | | |
| S38A | TA | 2283 | 1683 | 1320 | 2481 | 1641 | 1284 |
| S39A | TA | 2426 | 2035 | 2108 | 2358 | 1909 | 1904 |
| S40A | TA | 2559 | 2147 | 1993 | 2575 | 2314 | 2144 |
| S41A | TA | 1516 | 1118 | 1183 | 1938 | 1607 | 573 |
| S42A | TA | 2465 | 2363 | 2292 | 2831 | 2548 | 2633 |
| S43A | TA | 1473 | 940 | 764 | | 917 | |
| S44A | TA | 1688 | 2017 | 2087 | 1704 | 1977 | 2600 |
| S45A | TA | 1280 | 1216 | 1264 | 1099 | 1262 | 1440 |
| S46A | TA | 1251 | 1101 | 1169 | 1178 | 1351 | 1198 |
| S47A | TA | | 824 | | 952 | 847 | |
| S48A | TA | 2535 | 2426 | 2098 | 2479 | 2152 | 2093 |
| S49A | TA | 2027 | 2014 | 1624 | 2131 | 2436 | |
| S50A | TA | | | 2271 | 3190 | 3265 | 2304 |
| S51A | TA | 2331 | 2012 | 1091 | 1196 | 1209 | 1502 |
| S52A | TA | 3134 | 2998 | 2036 | 2703 | 2965 | 2499 |
| SCIA | US | | 241 | 279 | 182 | | |
| SFIN | TA | 1737 | 1095 | 550 | 2238 | 907 | 658 |
| T31A | TA | 1305 | 959 | 1052 | 1041 | | 915 |
| T32A | TA | 773 | 420 | | 613 | 440 | |
| T33A | TA | 1210 | 1019 | 1122 | 1076 | 1066 | 1079 |
| T34A | TA | 2114 | 1933 | 2116 | 1792 | 1960 | 2203 |
| T35A | TA | 1098 | 872 | 691 | 938 | 892 | 691 |
| T36A | TA | 1200 | 1327 | 1368 | 1448 | 1559 | 1542 |
| T37A | TA | 2087 | 1803 | 1562 | 2246 | 1911 | 1501 |
| T38A | TA | 2760 | 2710 | 2809 | 2945 | 2885 | 2828 |
| T39A | TA | 2843 | 2603 | 3285 | 2782 | 2806 | 3223 |
| T40A | TA | 2556 | 2716 | 2395 | 2728 | 2494 | 2216 |
| T41A | TA | 1504 | 2440 | 2265 | 1941 | 1681 | 1705 |
| T42A | TA | 2436 | 2010 | 1535 | 2426 | 2082 | 1502 |
| T43A | TA | 633 | 583 | 606 | 714 | 648 | 613 |
| T44A | TA | | 1279 | 462 | | | 926 |
| T45A | TA | | 579 | 1878 | 1065 | 759 | 1022 |
| T46A | TA | 2801 | | 3153 | 2853 | | |
| T47A | TA | 2184 | 1225 | 1850 | 2373 | 2459 | 2770 |
| T48A | TA | 2590 | 3302 | 2224 | 2764 | 3182 | |

| | | | | | | | |
|---|---|---|---|---|---|---|---|
| T49A | TA | 1455 | 2737 | | 3181 | 2624 | |
| T50A | TA | 2867 | 2726 | 2018 | 2350 | 2548 | 2604 |
| T51A | TA | 1766 | 1587 | 1449 | 1616 | 1646 | 1534 |
| TIGA | TA | | 1023 | | 1494 | | 687 |
| TUL1 | TA | 1345 | 1423 | 1421 | 1485 | 1626 | 1715 |
| TZTN | US | | | 3073 | 3330 | | |
| U30A | TA | | 349 | 403 | | 377 | 575 |
| U31A | TA | 508 | 416 | 490 | 388 | 430 | 542 |
| U32A | TA | 760 | 838 | 1085 | 745 | 838 | 1179 |
| U33A | TA | 1077 | 922 | 705 | 968 | 1009 | 786 |
| U34A | TA | 876 | 833 | 813 | 863 | 810 | 756 |
| U35A | TA | 1031 | 864 | 710 | 908 | 846 | 680 |
| U36A | TA | 1424 | 1208 | 1243 | 1517 | 1264 | 1384 |
| U37A | TA | 2571 | 2594 | 2485 | 2709 | 2571 | 2435 |
| U38A | TA | 2675 | 2529 | 2040 | 2833 | 2524 | 2268 |
| U39A | TA | 2780 | 2709 | 2541 | 3130 | 2970 | 2652 |
| U40A | TA | 2185 | 1853 | 1300 | 1853 | 2469 | 2332 |
| U41A | TA | 456 | 539 | 279 | 1057 | 734 | 808 |
| U42A | TA | 2958 | 2735 | 2443 | 3248 | 3184 | 3239 |
| U43A | TA | 319 | 316 | 276 | 657 | 703 | 741 |
| U44A | TA | 197 | | | 265 | | |
| U44B | TA | | 330 | 305 | 686 | 407 | 419 |
| U45A | TA | 410 | 243 | 250 | 253 | 209 | |
| U46A | TA | 675 | 517 | 425 | 372 | 636 | 509 |
| U47A | TA | 3048 | 1672 | 3188 | 2411 | | 3195 |
| U48A | TA | 3208 | 2677 | 2310 | 3263 | 3133 | 2660 |
| U49A | TA | 2989 | 2667 | 3281 | 3080 | 2788 | 3203 |
| U50A | TA | | 1253 | | | 1079 | |
| U51A | TA | 2984 | 2780 | | 2113 | 2433 | 1175 |
| U52A | TA | | | 1906 | | | |
| U53A | TA | 2277 | 2122 | | | | |
| V30A | TA | 344 | 432 | 549 | 482 | 407 | 488 |
| V31A | TA | 900 | 1103 | 1151 | 842 | 1087 | 799 |
| V32A | TA | 762 | 842 | 756 | 868 | 724 | 528 |
| V33A | TA | 1548 | 1350 | 1224 | 1411 | 1423 | 1120 |
| V34A | TA | 1142 | 1014 | 1056 | 1028 | 1021 | 1007 |
| V35A | TA | 678 | 490 | 502 | 582 | 510 | 537 |
| V36A | TA | 1356 | 1304 | 1274 | 1109 | 1330 | 1379 |
| V37A | TA | 2937 | 2890 | 2671 | 2941 | 2766 | 2521 |
| V38A | TA | 2128 | 2030 | 1343 | 2349 | 2355 | 1366 |
| V39A | TA | 1150 | 539 | 635 | 991 | 852 | 1013 |

| | | | | | | | |
|---|---|---|---|---|---|---|---|
| V40A | TA | 1791 | 1207 | 1108 | 1689 | 1154 | 1201 |
| V41A | TA | 1765 | 1114 | 1261 | 1196 | 1000 | 1068 |
| V42A | TA | 2593 | 2707 | 2172 | 2590 | 2137 | 2234 |
| V43A | TA | 205 | 290 | 256 | | 303 | 525 |
| V44A | TA | 107 | 95 | 177 | 127 | | 183 |
| V45A | TA | 373 | 225 | 256 | 322 | 283 | 253 |
| V46A | TA | 3208 | 2588 | 2684 | 3256 | | |
| V47A | TA | 3091 | 3020 | 687 | 2668 | | 1239 |
| V48A | TA | 3170 | | | 3443 | 3204 | |
| V49A | TA | | | | 3029 | 3131 | |
| V51A | TA | 3054 | 2013 | 2821 | 1327 | 2918 | 2594 |
| V52A | TA | 2793 | 3109 | | 2939 | 2626 | 1814 |
| V53A | TA | | | 2581 | 2296 | | |
| W30A | TA | 467 | 425 | 336 | 435 | | 527 |
| W31A | TA | 863 | 927 | 1310 | 628 | 852 | 929 |
| W32A | TA | 1166 | 1203 | 951 | 1170 | 1189 | 922 |
| W33A | TA | 1281 | 1189 | 1321 | 1130 | 1126 | 1220 |
| W34A | TA | 1037 | 883 | 765 | 1005 | 864 | 748 |
| W35A | TA | 641 | 529 | 480 | 657 | 515 | 482 |
| W36A | TA | 1294 | 1199 | 1147 | 1227 | 1133 | 1152 |
| W37A | TA | 2093 | 2049 | 1799 | 2161 | 2118 | 1637 |
| W37B | TA | 2408 | 2135 | 1894 | 2512 | 2553 | 2383 |
| W38A | TA | 1906 | 1866 | 1926 | 1899 | 1809 | 1989 |
| W39A | TA | 2443 | 2228 | 2185 | 2600 | 2351 | 2218 |
| W40A | TA | 1929 | 1533 | 1300 | 1700 | 1501 | 1219 |
| W41B | TA | 1645 | 2122 | 1940 | 1888 | 2352 | 1693 |
| W42A | TA | 563 | 285 | 579 | 693 | 516 | 474 |
| W43A | TA | 253 | | | 315 | | 124 |
| W45A | TA | 435 | 220 | 325 | 467 | 402 | 475 |
| W46A | TA | 645 | 605 | 336 | 1404 | 720 | 577 |
| W47A | TA | 1184 | 1042 | | | 1419 | 1739 |
| W48A | TA | 2556 | 2751 | 3247 | | | |
| W49A | TA | | 1992 | 3232 | | 3155 | 2859 |
| W50A | TA | 2668 | 2369 | 1818 | 2667 | 2638 | 3072 |
| W51A | TA | 3394 | | 2765 | | 2805 | 3255 |
| W52A | TA | 2559 | | | | | 2003 |
| W53A | TA | 2926 | | 1626 | 3051 | | 1352 |
| WHTX | TA | | 390 | 433 | 634 | 331 | |
| WMOK | US | 2843 | 2726 | 2689 | 2860 | 2828 | 2646 |
| X30A | TA | 1453 | 850 | 871 | 569 | 625 | 1040 |
| X31A | TA | 1041 | 1335 | 1859 | 1333 | 1715 | 2021 |

| | | | | | | | |
|---|---|---|---|---|---|---|---|
| X32A | TA | 1358 | 1326 | 1024 | 1490 | 1488 | 1001 |
| X33A | TA | 502 | 477 | 595 | 460 | 540 | 711 |
| X34A | TA | 1330 | 1176 | 1022 | 1310 | 1242 | 1035 |
| X35A | TA | 1406 | 1313 | 1288 | 1450 | 1437 | 1683 |
| X36A | TA | 1124 | 1032 | 728 | 1198 | 1096 | 829 |
| X37A | TA | 1852 | 1762 | 1668 | 1890 | 1861 | 1716 |
| X38A | TA | 1822 | 1875 | 1723 | 1987 | 1827 | 1667 |
| X39A | TA | 2879 | 2826 | 2936 | 2960 | 2778 | 2784 |
| X40A | TA | 2416 | 2189 | 1760 | 2174 | 1972 | 1758 |
| X41A | TA | 264 | 259 | | 633 | | |
| X42A | TA | 493 | 269 | 314 | 443 | 367 | 390 |
| X43A | TA | 187 | 185 | 163 | 104 | 108 | 165 |
| X44A | TA | 439 | 398 | 444 | 312 | 382 | 423 |
| X45A | TA | 679 | 603 | 737 | 703 | 569 | 734 |
| X46A | TA | 958 | 727 | 386 | 1770 | | |
| X47A | TA | | 992 | 1155 | 1630 | 1001 | 2680 |
| X50B | TA | | 2081 | 3164 | | | |
| X51A | TA | 3247 | | | | | |
| X53A | TA | 2946 | 3019 | | | 2736 | 2849 |
| Y30A | TA | 276 | 332 | 177 | | 277 | 369 |
| Y31A | TA | 1453 | 917 | 587 | 1693 | | |
| Y32A | TA | 744 | 755 | 807 | 808 | 808 | 868 |
| Y33A | TA | 980 | 1000 | 886 | 1046 | 1005 | 796 |
| Y34A | TA | 617 | 560 | 531 | 532 | 582 | 530 |
| Y35A | TA | 658 | 484 | 529 | 489 | 353 | 506 |
| Y36A | TA | 724 | 530 | 560 | 579 | 510 | 472 |
| Y37A | TA | 710 | 777 | 1024 | 647 | 762 | 919 |
| Y38A | TA | 916 | 869 | 965 | 1223 | 1051 | 1301 |
| Y39A | TA | 610 | 644 | 861 | 717 | 759 | 708 |
| Y40A | TA | 809 | 446 | 379 | 479 | 316 | 332 |
| Y41A | TA | 310 | 354 | 289 | 310 | 413 | 358 |
| Y42A | TA | 334 | 484 | 263 | 354 | 350 | 321 |
| Y43A | TA | | 92 | 76 | 326 | | 82 |
| Y44A | TA | 182 | | 182 | 220 | | 162 |
| Y45A | TA | 1268 | 987 | 1164 | 2347 | 507 | |
| Y46A | TA | 1087 | 817 | 986 | 1368 | 972 | 965 |
| Y47A | TA | | 1516 | 1175 | | | |
| Y50A | TA | | 830 | 558 | | | |
| Y52A | TA | 3073 | | 3219 | | | 3468 |
| Y53A | TA | | 1685 | 1517 | | 2584 | 2359 |
| Y54A | TA | | 2736 | 2875 | | | 3204 |

| | | | | | | | |
|---|---|---|---|---|---|---|---|
| Z31A | TA | 1431 | 1699 | 1041 | 1419 | 2019 | 2716 |
| Z32A | TA | 1494 | 1399 | 1683 | 1088 | 1586 | 1498 |
| Z33A | TA | 668 | 712 | 639 | 828 | 735 | 563 |
| Z34A | TA | 1048 | 913 | 870 | 1060 | 990 | 962 |
| Z35A | TA | 688 | 656 | 669 | 736 | 759 | 659 |
| Z36A | TA | 1290 | 1211 | 1104 | 1639 | 1528 | 1421 |
| Z37A | TA | 675 | 673 | 758 | 627 | 715 | 726 |
| Z38A | TA | 842 | 512 | 355 | 553 | 478 | 354 |
| Z40A | TA | 651 | 482 | | 592 | 604 | |
| Z41A | TA | 362 | 268 | 188 | 239 | 152 | |
| Z42A | TA | 223 | 190 | | | | |
| Z43A | TA | | | 257 | | | 341 |
| Z44A | TA | | | 108 | | | |
| Z45A | TA | | | | | | 362 |
| Z46A | TA | | 419 | 452 | | 281 | 192 |
| Z47A | TA | | | | | | 861 |
| Z48A | TA | | | 2973 | | | |
| Z52A | TA | | | | | | 3034 |